Article

Dynamical Simulation, Sensitivity, and Productivity Analysis of a Light-Photoacclimation Model for Microalgae-Based Carbohydrate Production in Continuous Photobioreactors

Abraham Guzmán-Palomino [1,†], Luciano Aguilera-Vázquez [1,*,†], Héctor Hernández-Escoto [2,†], Pedro Martin García-Vite [1,†] and Ana Lidia Martínez-Salazar [1,†]

[1] Tecnológico Nacional de México, Instituto Tecnológico de Ciudad Madero, Av. 1o. de Mayo esq. Sor Juana Inés de la Cruz S/N Col., Los Mangos, Ciudad Madero 89440, Mexico; d18073012@itcm.edu.mx (A.G.-P.); ana.ms@cdmadero.tecnm.mx (A.L.M.-S.)

[2] Departamento de Ingeniería Química, Universidad de Guanajuato, Guanajuato 36000, Mexico; hhee@me.com

[*] Correspondence: luciano.av@cdmadero.tecnm.mx; Tel.: +52-833-357-48-20

[†] These authors contributed equally to this work.

Abstract: The world's human population is increasing as is the demand for new sustainable sources of energy. Accordingly, microalgae-based carbohydrates for biofuel production are being considered as an alternative source of raw materials for producing biofuels. Microalgae grow in photobioreactors under constantly changing conditions. Models improve our understanding of microalgae growth. In this paper, a photoacclimated model for continuous microalgae cultures in photobioreactors was used to study the time-varying behavior and sensitivity of solutions under optimal productivity conditions. From the perspective of dynamic simulation in this work, light intensity was found to play an influential role in modifying metabolic pathways as a cell stressor. Enhancing carbohydrate productivity by combining nutritional deficiency and light intensity regulation modeling strategies could be helpful to optimize the process for the highest yield in large-scale cultivation systems. Under the proposed simulation conditions, a maximum carbohydrate productivity of 48.11 $gCm^{-3}d^{-1}$ was achieved using an optimal dilution rate of 0.2625 d^{-1} and 350 $\mu molm^{-2}s^{-1}$ of light intensity. However, it is important to note that, a particular set of manipulated inputs can generate multiple outputs at a steady state. A numerical solution of the sensitivity functions indicated that the model outputs were especially sensitive to changes in parameters corresponding to a minimum nitrogen quota, maximum nitrogen intake rate, dilution rate, and maximum nitrogen quota compared to to other model parameters.

Keywords: dynamic simulation; photoacclimation model; photobioreactors; microalgae; carbohydrate pool; sensitivity; productivity

1. Introduction

Global energy consumption is continuously rising due to the rapid growth of the world's population. As a consequence, the widespread use of fossil fuels worldwide has resulted in their depletion and near exhaustion due to their nonrenewable and nonsustainable nature [1,2]. In order to satisfy this energy demand, researchers are investigating the possibility of producing biofuels from biomass. Biomass refers to any organic matter capable of serving as an energy source [3]. This could includes wood, crops, and even garbage [4]. Nevertheless, the selection of appropriate feedstock for biofuel production plays a major role in the success of the process [5]. As bulk commodities, the production of biofuels requires abundant and cost-effective feedstocks, which are essential for the process to be economically viable, as well as other equally important social, environmental, geographical, and industrial factors [6,7]. Microalgae are considered to be more ecofriendly and sustainable energy sources due to their low emissions of greenhouse gases and other

pollutants [8]. Thus, the use of microalgae as a renewable source can also contribute to the mitigation of climate change [9–11]. In addition, microalgae require a fraction of the space required for most land-based energy crops; for example, producing algal biomass to meet 50% of the U.S. transport fuel demand would require only 1 to 3% of the total U.S. cropping area [12]. Moreover, microalgae have the advantage of being able to produce a larger amount of biomass in a shorter time compared to other sources. In fact, most strains are capable of doubling their cell mass in less than 24 h [13,14]. Within this context, microalgae have been found to be the most efficient organisms for converting sunlight into valuable energy-producing organic compounds; among the most important organic compounds in algae biomass are carbohydrates, proteins, and lipids [15–18]. Carbohydrates are the primary products of photosynthesis. In photosynthesis, nicotinamide adenine dinucleotide phosphate (NADPH) is utilized to fix and convert the carbon dioxide (CO_2) into glucose through a metabolic pathway known as the Calvin cycle. Although carbohydrates are lower in energy than other microalgae compounds, such as lipids, they are considered the most suitable material to produce biofuels by combining biotechnology with thermochemical conversion [19,20]. In general, biomass can be converted to energy through a variety of biological as well as thermochemical methods [21]. Biological conversion includes the fermentation of degradable substances to produce renewable energy sources, such as bioethanol, biobutanol, biohydrogen [22]. Accordingly, microalgae-based carbohydrates for biofuel production, are being considered as an alternative source of raw materials for producing biofuels [23–25]. Even though carbohydrates are lower in energy than are other microalgae compounds, such as lipids, they are considered to be the most suitable material for conversion into biofuels through a thermochemical conversion process since they contain a low level of lignin [26]. In light of this, microalgae-based carbohydrates are considered a promising alternative source of raw materials for the production of biofuels. The photobioreactor (PBR) is designed to convert luminous energy into valuable products. They are typically used in large-scale outdoor operations for the cultivation of microalgae and to provide precise control over the growth environment . There are four phases in a typical PBR: (1) solid phase (microalgal cells), (2) liquid phase (growth medium), (3) gaseous phase CO_2 and oxygen (O_2), and (4) a superimposed light-radiation field [27,28]. Moreover, microalgae cultures in photobioreactors (PBRs) are highly responsive to light intensity and require consistent light intensity to optimize biomass productivity and metabolic activity. Several types of PBRs have been developed so far, including bubble column, airlift reactor, flat-plate, stirred-tank, and tubular, among others [29,30]. There is a close relationship between light distribution, hydrodynamics, mass transfer, and growth kinetics that complicates the design process [31–33]. In-depth research efforts, especially those that combine theory and practice, remain necessary for the success of large-scale cultivation systems. Dynamic models are critical tools for optimizing and controlling microalgae-based carbohydrate systems in the laboratory and on large scales. Dynamic models are of utmost importance in achieving optimal carbohydrate production and other valuable metabolites in microalgae. To bridge the gap between theoretical predictions and industrial photosynthetic productivity, it is vital to identify the limiting factors that impact the conversion of light energy into biomass. This understanding allows for the development of effective strategies to optimize microalgae production and align theoretical insights with practical implementation [34–36]. Over the past decade, a variety of mathematical models that describe the growth kinetics of microalgae have been developed to understand their application in large-scale microalgae production [37]. These models examine the influence of process parameters such as light, temperature, nutrients, oxygen concentration, salinity, pH, and organic or inorganic carbon on microalgae growth rates [38]. In most of the models, these conditions change over time, and the effects of these variations on growth are not considered; these variations are extremely important factors to be investigated in order to address large-scale problems [39] and constitute the frontier of knowledge and the contribution to research. Photobioreactors are characterized by multivariable conditions for microalgae cultivation. The physical, chemical, and biological processes occurring inside

a photobioreactor are difficult to study because most of them take place simultaneously and are strongly interdependent. Proper control of the environmental variables governing these processes is essential to the successful design and operation of a photobioreactor [40]. As mentioned above, few parameters are nearly constant; as a result, identifying the parameters that have the greatest impact on the model through sensitivity analysis can help determine which parameters are most critical during parameter calibration [41,42]. In this study, a dynamic photoacclimated model for continuous microalgae culture systems was used to study time-varying state variables behavior as well as the first-order effects of solutions to parameter variations under optimal productivity conditions. To this end, it was crucial to recognize that the productivity of a photobioreactor is largely determined by the dynamic control of its environmental factors. Additionally, having a thorough understanding of how model sensitivities vary during different phases of growth can help to significantly improve their efficiency and productivity.

1.1. Dynamic Photoacclimation Model

New techniques from biotechnology and the control field are necessary for large-scale microalgal cultivation to ensure robustness, durability, and optimization of the process. A critical challenge in converting solar light energy into chemical energy is providing sufficient light to sustain cell growth. As biomass concentration increases, so does light absorption. However, the maximal biomass attainable is limited by a critical biomass concentration, where all impinging photons are absorbed . The limitation to achieving a high biomass yield in microalgal cultivation is not a straightforward matter, as it is affected by the adaptive mechanism of cells to optimize light harvesting through pigments [43]. The concentration of pigments is dependent on light intensity, which in turn determines light attenuation. Moreover, an excess of photons can cause irreversible damage to a key protein involved in the photosystem II reaction centers in the chloroplasts, leading to photodamage and photoinhibition. These challenges require the development of new modeling and control strategies for microalgal-based processes. Specific dynamic models have been designed to understand and model this process, taking into account the close relationship between photoinhibition and photoacclimation [44]. Geider et al. [45] were the pioneers in proposing a simple model that includes chlorophyll (Chl) as a variable, along with microalgal carbon and nitrogen, to account for the response of photosynthesis to light and nitrogen status [46]. From this model, other models have been proposed [47]. These additional models aim to improve the understanding of microalgae behavior and optimize their biomass production. The primary characteristic of these models is the process of photoacclimation, which enables the microalgae to adjust the synthesis of pigments, particularly chlorophyll, in response to changes in light intensity [47–50]. One of the main challenges in the development of microalgal models is their calibration, validation, and application for control purposes. Despite these challenges, these models have a crucial role in enhancing our understanding of microalgal behavior and optimizing their growth and biomass production.

In this study, a dynamic model explaining photoinhibition and photoacclimation was used [51–53]. The model employs the classical Droop expression [54]. In a photobioreactor, the Droop equations describe the growth of microorganisms by combining three coupled, nonlinear ordinary differential equations. The Droop model uncouples growth from substrate uptake, resulting in defining an internal cell quota (i.e., the amount of internal nutrients present in each unit of biomass), which determines growth rate. The amount of nutrients taken up by cells is determined by the external concentration of nutrient y (nitrogen) [55]. The subsistence quota restricts algae growth below a certain amount. The photon flux density of photoacclimation is introduced as a state variable, I^*, to represent the light intensity of photoacclimation at a given physiological level [56]. The model proposed in [56,57] presents an analytical integration based on the average growth rate of the entire culture. This model, in its simplified form, has potential for process control, especially when the expression of photoinhibition is changed to a Haldane-inhibitory formulation.

A microalgae photobioreactor is a complex system, primarily due to its nonlinear and time-varying behavior, and most studies do not account for photoacclimation, so it would be valuable to examine its dynamic behavior.

By incorporating the mathematical description of photoacclimation and applying appropriate kinetic expressions for the nitrogen intake rate (ρ) and the specific growth rate (μ), the Droop's mass balance differential equation for biomass x, substrate y, and intracellular nitrogen quota z are determined for an assumed perfectly mixed PBR [56,58,59]; the model nomenclature is described in detail in Table 1.

$$
\begin{aligned}
\dot{x} &= \mu(x, z, I_0)x - Dx - Rx \\
\dot{y} &= Dy_{in} - \rho(y, z)x - Dy \\
\dot{z} &= \rho(y, z) - \mu(x, z, I_0)(z - zc_0) + Rz \\
\dot{I}^* &= \mu(x, z, I_0)[\bar{I}(I_0) - I^*]
\end{aligned}
\tag{1}
$$

In this equation, D is the dilution rate (the ratio of the flow rate of the influent over the volume of the photobioreactor), and Dy_{in} is the influent nutrient concentration of nitrate in the influent. The respiration rate is expressed by R. The uptake rate assumed in this model corresponds to that defined by the Michaelis–Menten law, and the specific growth rate is expressed in terms of the intracellular nitrogen quota (z) [54–56,58,60]. In order to calculate the remaining parameters of the model, the expressions in (2)–(11) are used.

Table 1. List of Functions, State Variables, and Parameter Nomenclature.

Functions	Definition	Unit
μ	Specific growth rate	gCm^{-3}
$\bar{\mu}$	Maximum specific growth rate	gNm^{-3}
k_{sI}	Normalized growth half saturation constant	$gN(gC)^{-1}$
θ	Chlorophyll quota	$gChl(gC)^{-1}$
ξ	Light-attenuation rate light-attenuation coefficient	d^{-1}
λ	Optical depth	m^{-1}
Chl	Chlorophyll concentration	gCm^{-3}

State variables	Definition	Unit
x	Biomass concentration	gCm^{-3}
y	External nutrient concentration	gNm^{-3}
z	Intracellular nitrogen quota	$gN(gC)^{-1}$
I^*	Photon flux density acclimation	$\mu mol m^{-2}s^{-1}$
q_g	Carbohydrate quota	$gC(gC)^{-1}$

Parameters	Definition	Unit
I_0	Light intensity	$\mu mol m^{-2}s^{-1}$
D	Dilution rate	d^{-1}
y_{in}	Nitrogen concentration in the reactor inlet	gNm^{-3}
$\bar{I}$	Average photon flux density throughout the culture	$\mu mol m^{-2}s^{-1}$
ρ	Nitrogen intake rate	$gN(gC)^{-1}d^{-1}$
ρ_m	Maximum specific growth rate	$gN(gC)^{-1}d^{-1}$
k_s	Substrate-uptake half-saturation constant	gNm^{-3}
$k_{sI}{}^*$	Growth half-saturation constant	$\mu mol m^{-2}s^{-1}$
k_{iI}	Photon flux density saturation constant over growth	$\mu mol m^{-2}s^{-1}$
γ	Chlorophyll saturation function	$gChl(gN)^{-1}$
γ_m	Maximum chlorophyll saturation function	$gChl(gN)^{-1}$
k_{I^*}	Chlorophyll saturation function constant	$\mu mol m^{-2}s^{-1}$
K_g	Average photon flux density saturation function constant	$-$
L	Culture depth	m
a	Attenuation coefficient due to chlorophyll	$m^2(gChl)^{-1}$
b	Attenuation coefficient due to biomass	$m^2(gC)^{-1}$
c	Attenuation coefficient due to background turbidity	m^{-1}
α	Protein synthesis coefficient	$gC(gN)^{-1}$
β	Fatty acid synthesis coefficient	$gC(gN)^{-1}$
zc_m	Maximum nitrogen quota	$gN(gC)^{-1}$
zc_0	Minimum nitrogen quota	$gN(gC)^{-1}$
R	Respiration rate	d^{-1}

1.1.1. Specific Growth Rate

The specific growth rate is recalled from [56] in order to take into account the light intensity.

$$\mu(x, z, I_0) = \bar{\mu}(I)\left(1 - \frac{z_0}{z}\right) \tag{2}$$

$$\bar{\mu}(I) = \tilde{\mu}\frac{I}{I + K_{sI} + \frac{I^2}{K_{il}}} \tag{3}$$

$$k_{sI} = \frac{k_{sI*}}{\theta} \tag{4}$$

$$\theta = \frac{Chl}{x} \tag{5}$$

$$\xi = aChl + bx + c \tag{6}$$

$$\lambda = \xi L \tag{7}$$

$$Chl = \gamma(I^*)xz \tag{8}$$

$$\gamma(I^*) = \gamma_m \frac{k_{I*}}{k_{I*} + I^*} \tag{9}$$

1.1.2. Nutrient Uptake

According to the Michaelis–Menten law, the uptake rate can be defined as follows:

$$\rho(y, z) \quad = \quad \rho_m \frac{y}{y + k_y}\left(1 - \frac{z}{zc_m}\right) \tag{10}$$

For modeling the time evolution of this additional variable, Beer–Lambert expressions for the absorbance of light in the culture medium have been proposed [60]. The average light irradiation (i.e., the photon flux density that affects the culture mass on average) is calculated with $\bar{I}$ and is used to drive the dynamics of the acclimation phenomenon through a factor proportional to $(\bar{I}-I^*)$ [58].

1.1.3. Average Photon Flux Density throughout the Culture

$$\bar{I} \approx I_0 \frac{K_g}{\lambda + K_g} \tag{11}$$

1.2. Carbon Flux and Carbohydrates Dynamics

In order to explain how nitrogen limitations affect carbohydrate and neutral lipid accumulations, Mairet [57] has proposed a dynamical model based on a simplified carbon metabolism, as shown in Figure 1.
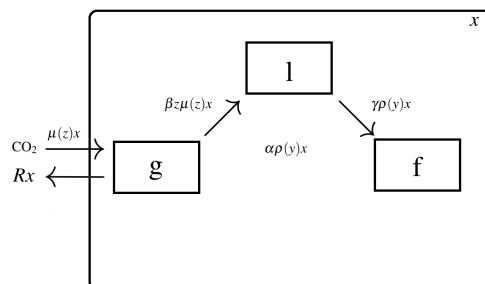

Figure 1. Metabolic route for carbohydrate dynamics.

First, carbon dioxide is shown to be incorporated into a carbohydrate pool. These carbohydrates are mobilized by microalgae to produce proteins and nucleic acids, which

are dependent on nitrogen. Moreover, the carbohydrate compartment (g) is used in a parallel pathway to synthesize free fatty acids (FFAs). The rate of fatty acid synthesis is determined by the rate of photosynthesis, as well as the nitrogen quota. Further, the FFAs may either be stored as neutral lipids (l) or mobilized for the purpose of creating functional carbon (f) (membranes) [56,57].

Carbohydrate Dynamics Deduction

On the basis of the previously described simplified metabolic network shown in Figure 1, the dynamics of carbohydrate production could be derived as follows:

$$\dot{g} \quad = \quad (1 - \beta z)\mu(x, z, I_0)x - \alpha\rho(y, z)x - Dg - Rx \tag{12}$$

As shown in Figure 1, biomass (x) is composed of functional carbon (f), carbohydrates (g), and lipids (l). Based on this information, Equation (13) represents the sum of these three sources of carbon:

$$x = f + g + l \tag{13}$$

Based on the above, the proportion that corresponds to the carbohydrate share of total biomass can be calculated as follows: (14)

$$q_g = \frac{g}{x} \tag{14}$$

By dividing both sides of Equation (12), Equation (15) becomes

$$\frac{\dot{g}}{x} \quad = \quad \frac{(1 - \beta z)\mu(x, z, I_0)x}{x} - \frac{\alpha\rho(y, z)x}{x} - D\frac{g}{x} - \frac{Rx}{x} \tag{15}$$

By solving D of (1) in steady state, we obtain Equation (16) as follows:

$$D \quad = \quad \mu(x, z, I_0) - R \tag{16}$$

By substituting the value of D into Equation (15), Equation (17) is obtained as follows:

$$\frac{\dot{g}}{x} \quad = \quad (1 - \beta z)\mu(x, z, I_0) - \alpha\rho(y, z) - (\mu(x, z, I_0) - R)\frac{g}{x} - R \tag{17}$$

Substituting $\frac{\dot{g}}{x}$ for $\dot{q}_g$ and $\frac{g}{x}$ for q_g in Equation (17) results (18) in the following:

$$\dot{q}_g \quad = \quad (1 - \beta z)\mu(x, z, I_0) - \alpha\rho(y, z) - (\mu(x, z, I_0) - R)q_g - R \tag{18}$$

This Equation (18) can be simplified to provide the following Equation (19), which describes the dynamics of the carbohydrate quota:

$$\dot{q}_g \quad = \quad (1 - \beta z - g_q)\mu(x, z, I_0) - \alpha\rho(y, z) + R(q_g - 1) \tag{19}$$

2. Materials and Methods

2.1. The Fermentation Process Simulation

Photobioreactors have been designed to produce high algal biomass density and rapid multiplication at a low cost [27]. The representation shown in Figure 2 illustrates the main inputs and outputs of the microalgae photobioreactor considered in this report.

The fermentation process simulation described in this study aims to model and analyze the dynamic behavior of microalgae cultivation. The simulation utilizes a photobioreactor (PBR) in which, instead of a sole reliance on the absolute volume of the reactor, the control parameter chosen for this simulation is the dilution rate. By employing the dilution rate as a control parameter, the simulation addresses concerns related to reactor scale. The

dilution rate provides a more meaningful measure of the rate of dilution and medium renewal, allowing for better control and optimization of the fermentation process. It enables precise adjustments of nutrient concentration and other critical parameters throughout the simulation, ensuring accurate representation of the actual conditions.
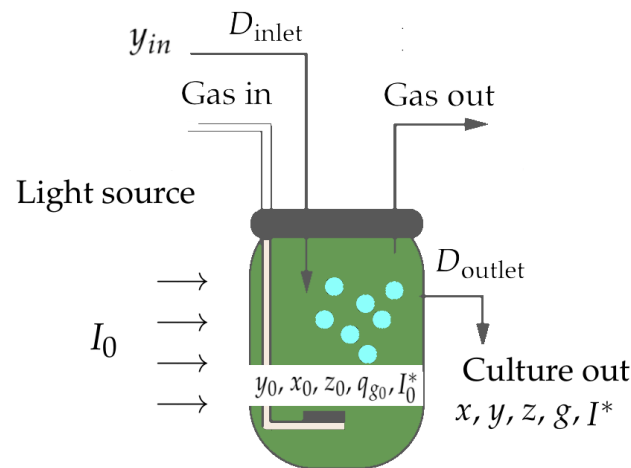

Figure 2. Conceptual illustration of the cultivation of microalgae in a continuous photobioreactor system. The variables y, x, z, q_g, and I^* represent external nutrients, biomass, intracellular nitrogen quota, carbohydrate quota, and photoacclimation respectively. The dilution rate and initial light intensity are given by D and I_0, respectively.

Meanwhile, the influent nutrient concentration (y_{in}) in the simulation of the fermentation process refers to the concentration of nutrients in the culture medium or input medium before cells initiate growth, as depicted in Figure 2. This concentration can either remain constant or vary over time depending on the experimental design or system conditions. In this study, the variable (y_{in}) was set to be equal to the initial concentration of the external nutrient (y_0), which represents the nutrient concentration within the microalgal cells at the beginning of the cultivation.

2.1.1. Methodology for Dynamic Simulation

Summarizing, the PBR model (1)–(19) describes the evolution of biomass and the ones of carbohydrates and photoacclimation factor, and prompts the close coupling between these states. This model enables the analysis of the effect of light in biomass and carbohydrate production, which is carried out in the following. The effect of nutrients has been examined in several other studies with only Droop-type models The set of ordinary differential equations (ODEs) of the model was solved through a solver called LSODE in GNU Octave version 7.1.0. The methods included for numerical solution can be found in [61]. The model parameters are given in Table 2, which were recalled from [56,58] to simulate the cultivation of *Isochrysis galbana* strain.The initial conditions for the Droop model were estimated using data obtained from culture runs reported in [58]. These runs involved simulations with the Droop model, which was also utilized in this study. The collected experimental data were utilized for parameter identification and cross-validation tests. The measured state variables in [58], including biomass concentration, intracellular nitrogen quota, external nutrient concentration, and chlorophyll concentration, were analyzed along with their corresponding 95% confidence intervals. These experimental results were compared to the model predictions based on the identified parameters, allowing for a visual comparison. By incorporating the identified parameters and comparing the experimental and model results, more realistic initial conditions for the state variables could be established for the dynamic simulation analysis in this study. Additionally, the initial condition for the carbohydrate quota was estimated using simulations from a previous study [62].

Table 2. Model parameters for simulating the cultivation of *Isochrysis galbana* [56,58].

Parameter	Value	Unit
$\tilde{\mu}$	1.7	d^{-1}
k_y	0.0012	gNm^{-3}
zc_0	0.05	$gN(gC)^{-1}$
zc_m	0.25	$gN(gC)^{-1}$
ρ_m	0.073	$gN(gC)^{-1}$
k_{sI}^*	1.4	$\mu molm^{-2}s^{-1}$
k_{iI}	295	$\mu molm^{-2}s^{-1}$
R	0.0081	d^{-1}
γ_m	0.57	$gChl(gN)^{-1}$
k_I^*	63	$\mu molm^{-2}s^{-1}$
a	16.2	$m^2(gChl)^{-1}$
b	0.087	$m^2(gChl)^{-1}$
c	0	m^{-1}
K_g [1]	10.6	$-$
α	2.6	$mgC(mgN)^{-1}$
β	4.8	$mgC(mgN)^{-1}$

[1] Parameter taken from [58].

In order to analyze the effect of light intensity, the analysis of equilibrium and productivity, as well as a parameter sensitivity analysis, were carried out considering four scenarios of light intensity, as show in Table 3. Considering the light-intensity constant was first methodological study step.

Table 3. Scenarios of initial light intensity for continuous photobioreactor simulations of *Isochrysis galbana* strain growth.

Simulation Scenario	Initial Light Intensity (I_0) [1]	Unit
A	50	$\mu molm^{-2}s^{-1}$
B	150	$\mu molm^{-2}s^{-1}$
C	250	$\mu molm^{-2}s^{-1}$
D	500	$\mu molm^{-2}s^{-1}$
E	750	$\mu molm^{-2}s^{-1}$

[1] Simulated under constant initial light intensity.

2.1.2. Methodology for Equilibrium and Productivity Analysis

Biomass productivity has long been recognized as a key indicator of continuous bioreactor performance. In this section, we leverage the model's capability to accurately describe carbohydrate accumulation to identify the optimal operational parameters, namely light intensity and dilution rate. By doing so, we can simulate and attain a maximum carbohydrate yield under the specific conditions outlined in this study. The resulting productivity values are then employed as nominal parameters in our comprehensive sensitivity analysis. Equations (20) and (21) illustrate the calculation of diagrams showing the equilibria and productivity of biomass (x) and carbohydrates (g) in relation to simulations that vary the parameters of light intensity and dilution rate. The simulation was conducted for a period of 100 days. The calculation of biomass and carbohydrate productivity was carried out by computing the following equations:

$$P_C = \vec{x}\vec{D} \tag{20}$$

$$P_g = \vec{x}\vec{q_g}\vec{D} \tag{21}$$

P_C is the biomass productivity curve, and P_g is the carbohydrate productivity curve. $\vec{x}$ represents the vector of solutions for biomass at steady state. The expression $\vec{D}$ represents the range of dilution rates from 0.02 to 0.5 with increments of 0.02 units. There was a range

of variation between 50 and 1000 molm^{-2}s^{-1} with increments of 25 units . A vector of carbohydrate quota solutions at a steady state is denoted as $\vec{q_g}$, which is obtained from simulations of a continuous culture system using the *Isochrysis galbana* strain. The data used for these simulations are presented in Table 2.

2.1.3. Methodology for Sensitivity Analysis

To provide first-order estimates of the effect of parameter variations on the state variables solutions, the sensitivity function (22) was solved by the following steps [63]: First, the nominal state equation was solved for nominal parameters. Then, the Jacobian matrices (23) and (24) of the considered model were calculated and evaluated. Finally, the sensitivity equations were numerically solved using Equation (25).

The function $S(t)$ is called a sensitivity function, and (22) is called a sensitivity equation. The nomenclature list is shown in Table 4.

$$\dot{S}(t) \quad = \quad A(t, \lambda_0)S(t) + B(t, \lambda_0) \tag{22}$$

where:

$$A(t, \lambda) = \left. \frac{\partial f(t, x, \lambda)}{\partial x} \right|_{x = x(t, \lambda)} \tag{23}$$

$$B(t, \lambda) = \left. \frac{\partial f(t, x, \lambda)}{\partial \lambda} \right|_{x = x(t, \lambda)} \tag{24}$$

$$\begin{aligned} \dot{x}_1 &= f(t, x, \lambda) & x(t_0) &= x_0 \\ \dot{x}_\lambda &= \left[\frac{\partial f(t, x, \lambda)}{\partial x} \right] x_\lambda + \left[\frac{\partial f(t, x, \lambda)}{\partial \lambda} \right] & x\lambda(t_0) &= 0 \end{aligned} \tag{25}$$

Table 4. Nomenclature list of symbols used in the sensitivity function.

Symbol	Definition
$S(t)$	Sensitivity function
x	State variables
λ	System evaluated parameters
λ_0	Nominal value of λ
A	First-order partial derivatives with respect to x
B	First-order partial derivatives with respect to λ

The aforementioned sensitivity function enables us to estimate the first-order effect of parameter variations on solutions. Additionally, it can be used to approximate the solution when the parameter λ is sufficiently close to its nominal value λ_0. A Taylor series expansion around the nominal solution $x(t, \lambda_0)$ can be used to obtain a good approximation for small values of $\|\lambda - \lambda_0\|$, as shown in Equation (26) [63].

$$x(x, \lambda) \quad = \quad x(t, \lambda_0) + S(t)(\lambda - \lambda_0) + \text{higher order terms} \tag{26}$$

By neglecting the higher-order terms [63], the solution $x(t, \lambda)$ can be approximated as follows:

$$x(x, \lambda) \quad \approx \quad x(t, \lambda_0) + S(t)(\lambda - \lambda_0) \tag{27}$$

Equation (27) is the first-order approximation of the differential equation and serves as the foundation for the procedure. A more detailed explanation and justification for this approximation can be found in [63]. The approximation is valid if the differential equations are differentiable and continuous, satisfying the existence and uniqueness theorem [42,63]. In this context, sufficient conditions for the existence and uniqueness of the Droop model have been established in previous studies, such as in [64].

To calculate the sensitivity, it is convenient to rename the parameters and state variables in Equation (1). One of the simplest approaches is to define the aforementioned parameters and variables as follows:

The arrangement (28) is a representation of the parameters represented by the symbol (λ), and the array (29) is a representation of the nominal parameters (λ_0).

$$
\lambda = \begin{bmatrix} \lambda_1 & \lambda_6 & \lambda_{11} \\ \lambda_2 & \lambda_7 & \lambda_{12} \\ \lambda_3 & \lambda_8 & \lambda_{13} \\ \lambda_4 & \lambda_9 & \lambda_{14} \\ \lambda_5 & \lambda_{10} & \lambda_{15} \end{bmatrix} = \begin{bmatrix} D & K_{iI} & \alpha \\ I_0 & \rho_m & \beta \\ \gamma_m & K_S & a \\ K_{sI}^* & zc_m & b \\ K_{I*} & zc_0 & k_g \end{bmatrix}
\tag{28}
$$

$$
\lambda_0 = \begin{bmatrix} \lambda_{0_1} & \lambda_{0_6} & \lambda_{0_{11}} \\ \lambda_{0_2} & \lambda_{0_7} & \lambda_{0_{12}} \\ \lambda_{0_3} & \lambda_{0_8} & \lambda_{0_{13}} \\ \lambda_{0_4} & \lambda_{0_9} & \lambda_{0_{14}} \\ \lambda_{0_5} & \lambda_{0_{10}} & \lambda_{0_{15}} \end{bmatrix} = \begin{bmatrix} D_0 & K_{iI_0} & \alpha_0 \\ I_{0_0} & \rho_{m_0} & \beta_0 \\ \gamma_{m_0} & K_{s_0} & a_0 \\ K_{sI_0^*} & zc_{m0} & b_0 \\ K_{I_0^*} & zc_{0_0} & k_{g_0} \end{bmatrix}_{\text{nominal}}
\tag{29}
$$

The arrangement (30) presents the nomenclature of the variables involved in the sensitivity analysis.

$$
x = \begin{bmatrix} \dot{x}_1 \\ \dot{x}_2 \\ \dot{x}_3 \\ \dot{x}_4 \\ \dot{x}_5 \end{bmatrix} = \begin{bmatrix} \dot{x} \\ \dot{y} \\ \dot{z} \\ \dot{I}^* \\ \dot{g}_q \end{bmatrix}
\tag{30}
$$

By using the lsode function in GNU Octave v. 7.1.0, sensitivity equations were computed and simulated using the nominal parameters shown in Table 2.

The initial conditions of the above renamed state variables x_{10}, x_{20}, x_{30}, x_{40}, and x_{50} for the simulation of the Droop model's sensitivity functions in a continuous culture system of *Isochrysis galbana* strain are shown in Table 5. It is worth noting that the dynamic simulations in Section 3.1 were performed using the initial conditions corresponding to (C_1) as shown in Table 5.

Table 5. The initial conditions of state variables x_{10}, x_{20}, x_{30}, x_{40}, and x_{50} for the simulation of the Droop model's sensitivity functions in a continuous culture system of *Isochrysis galbana* strain.

Initial Conditions	x_{10}	x_{20}	x_{30}	x_{40}	x_{50}
C_1	10.1	33.2	0.055	50	0.3
C_2	30.7	41.3	0.055	50	0.3
C_3	225	49.9	0.055	50	0.3

3. Results and Discussion

3.1. Dynamics Simulation

According to the FBR model presented in the Equations (1)–(19), this section presents the simulation results and analysis of the time-varying behavior of the light-photoacclimation model.

Figure 3 illustrates the time-varying behavior of biomass concentration and external nutrient concentration under different scenarios of light intensity shown in Table 3.

Figure 3b illustrates that scenario A achieved a lower steady-state biomass concentration (448.78 gCm^{-3}) than did scenarios B, C, D, and E, corresponding to 539.65, 558.12, 558.86, and 544.54 gCm^{-3}, respectively. In scenario B, the biomass concentration was higher than was the concentration obtained in scenario A. As compared to scenario B, scenario C had a higher biomass concentration. Considering the highest specific growth rate reached during the simulation of scenarios B and C, there was a difference of 47.19%.
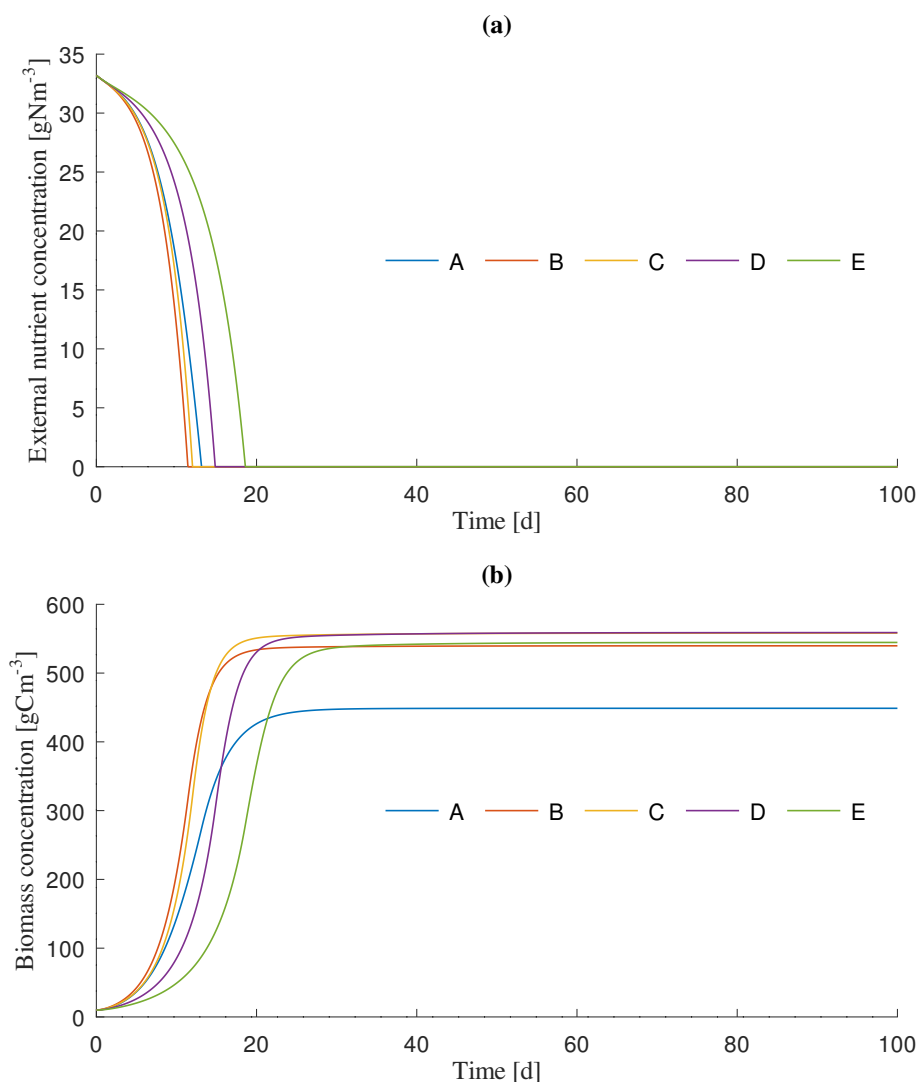
Figure 3. Simulation of (**a**) external nutrient concentration and (**b**) biomass concentration in a continuous culture system of microalgae of the *Isochrysis galbana* strain. The simulation input parameters are presented in Table 2 and the initial conditions in Table 5. The light intensity settings for A, B, C, D, and E correspond to 50 μmolm^{-2}s^{-1}, 150 μmolm^{-2}s^{-1}, 250 μmolm^{-2}s^{-1}, 500 μmolm^{-2}s^{-1}, and 750 μmolm^{-2}s^{-1}, respectively.

Additionally, based on simulations conducted in scenarios D and E, an increase in light intensity led to a a slight reduction in biomass concentration (2.56%) and growth rates (11.81%). Despite the fact that the concentration reached in the steady state in scenario D did not differ significantly from that found in scenario C, a a slight reduction in growth rate (6.86%) was observed in scenario D compared to scenario C. Each simulation case maintained a constant initial concentration of biomass and nutrients. Similar findings were reported in a previous study [65], where it was observed that while growth saturation was rapidly achieved at irradiance levels exceeding 200 μmolm^{-2}s^{-1}, no indications of photoinhibition were observed, even at higher irradiance levels of up to 400 μmolm^{-2}s^{-1}. The findings of our study are consistent with the research conducted by Sukenik and Wahnon (1991) [66] and by Tzovenis et al. (2003) [67]. These studies also reported that growth saturation occurred at irradiance levels above 300 and 200 μmolm^{-2}s^{-1}, respectively, and no photoinhibition was observed until a light intensity of μmolm^{-2}s^{-1} [67]. These findings highlight the robustness and reproducibility of the observed growth saturation phenomenon and the absence of photoinhibition under the specified irradiance conditions. These results suggest that our simulation outcomes are in line with the existing

literature and contribute to our understanding of the growth and photoinhibition dynamics of microalgae under varying light conditions.

Figure 3a illustrates that the concentration of external nutrients was removed more rapidly in scenario B ($0.056 \, \text{gN(gC)}^{-1}\text{d}^{-1}$) than in scenarios A, C, D, and E.

As a result, the biomass was obtained at a faster growth rate than that in any other scenario, as shown in Figure 3b. However, as indicated in Figure 3a, in the exponential growth phase, scenario C resulted in a 14.3% slower consumption of external nutrients compared to scenario B despite a higher metabolization of the nutrient as biomass. These results suggest that although microalgae depend on light for photosynthesis and energy production, excessive light intensity can negatively impact their nutrient intake and metabolism. Therefore, it is essential to optimize the light conditions in microalgae cultures to promote efficient nutrient utilization and enhance overall growth and productivity. Furthermore, the rate at which the nutrient concentration was depleted was significantly affected by the intensity of the light, as shown in scenarios D and E in Figure 3a. Essentially, the mathematical simulation indicated that light affects the efficiency of photosynthetic energy capture to assimilate and metabolize nitrogen from the external culture medium. Furthermore, a decrease in nitrate concentration leads to a significant reduction in biomass content, indicating that nitrogen starvation negatively affects the metabolic activity and cell division in *I. galbana*. These findings are consistent with previous studies [68,69]. In microalgae culture systems, nutrient and carbon utilization are closely linked. In order to generate energy from stored carbon, microalgae use the tricarboxylic acid cycle. As a result of this energy, inorganic nitrogen (ammonium) is absorbed to produce glutamine and glutamate amino acids, which require energy in the form of ATP and NADPH, as well as carbon skeletons in the form of 2-oxoglutarate and oxaloacetate [70,71].

These results are consistent with the previous literature highlighting the importance of nitrogen in various biological macromolecules, such as proteins, chlorophyll, photosystems, enzymes, and genetic materials [72,73]. Nitrogen deprivation has been identified as a significant limiting factor that impacts both growth and biomass production [74,75]. Studies have observed that a lack of nitrogen leads to a decrease in the synthesis of photosynthetic pigments, which subsequently hampers the processes of photosynthesis and assimilation [76,77]. Therefore, our findings support the notion that light plays a critical role in the efficiency of photosynthetic energy capture for nitrogen assimilation from the external culture medium.

The mathematical simulation illustrated in the Figure 4 showed that the dynamic behavior of the assimilation of the intracellular nitrogen quota (*z*) varied with the illumination conditions used in each scenario. It was observed that the internal quota of nutrients increased in scenarios of higher light intensity (D and E), achieving a maximum saturation value as the external nutrient concentration decreased. In addition, the simulation indicated that once external nutrients were removed from the culture medium, the cells began to metabolize the nitrogen that the cells had stored.
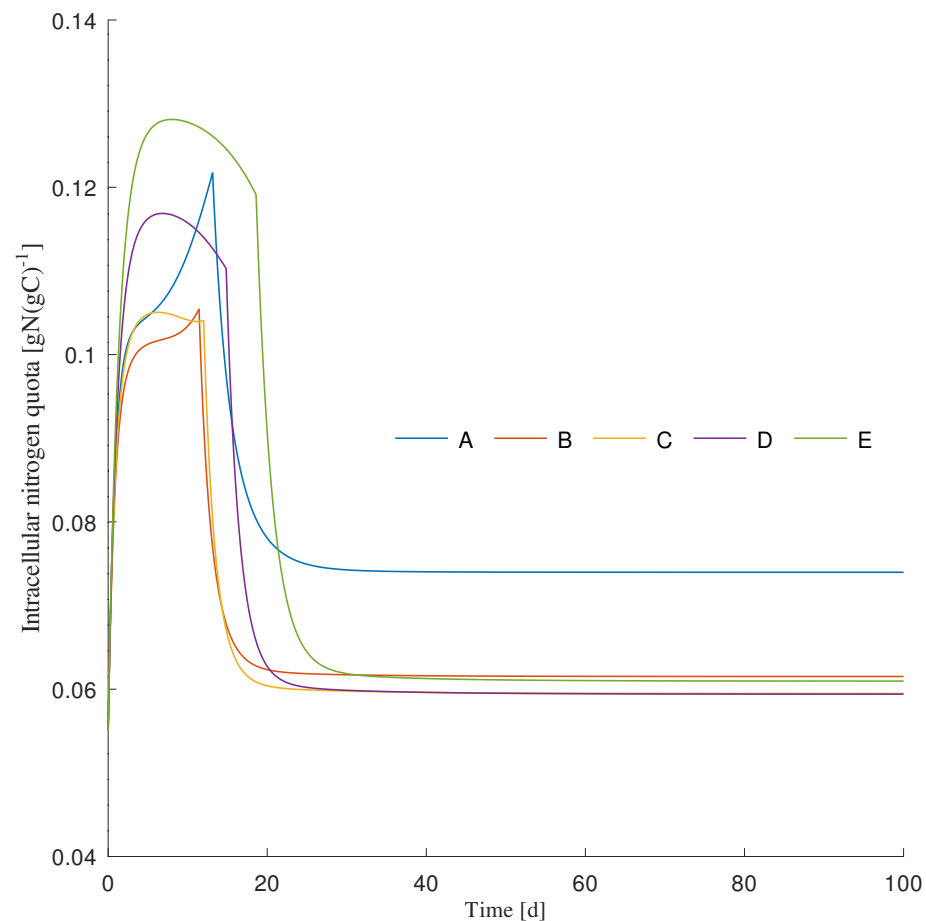
Figure 4. Simulation of internal nutrient quota in a continuous culture system of microalgae of the *Isochrysis galbana* strain. The simulation input parameters are presented in Table 2 and the initial conditions in Table 5. The light intensity settings for A, B, C, D, and E correspond to 50 μmolm^{-2}s^{-1}, 150 μmolm^{-2}s^{-1}, 250 μmolm^{-2}s^{-1}, 500 μmolm^{-2}s^{-1}, and 750 μmolm^{-2}s^{-1}, respectively.

Meanwhile, Figure 5 illustrates the results of a dynamic simulation of photoadaptation and chlorophyll concentration under different light-intensity conditions.

The photoacclimation dynamics described by (I^*), varied according to the simulated light-intensity scenarios. As can be observed in Figure 5a, the greater the intensity of incident light in the photobioreactor was (I_0), the greater the degree of photoacclimation. Conversely, as shown in Figure 5b, the higher the intensity of incident light in the photobioreactor was, the lower the chlorophyll concentration. In Figure 5b, it can be seen that in scenario A, the concentration of chlorophyll was higher over time than in any other scenario. In scenario E, there was a lower concentration of chlorophyll than in any other scenario. In accordance with the literature, the dynamic behavior observed in this study provides a consistent description of the photoacclimation mechanism [56]. The photoacclimation is the process by which chlorophyll synthesis is adapted to the intensity of light. There is a strong dynamic correlation between chlorophyll concentration and nutrient removal [78]. In order to maximize their ability to absorb light energy from sources of light, microalgae tend to produce a higher concentration of chlorophyll during low lighting conditions as shown in scenario A.

According to the results of the mathematical simulation of the carbohydrate quota in Figure 6a, scenario C had a higher carbohydrate quota concentration than did scenarios A, B, D, and E.
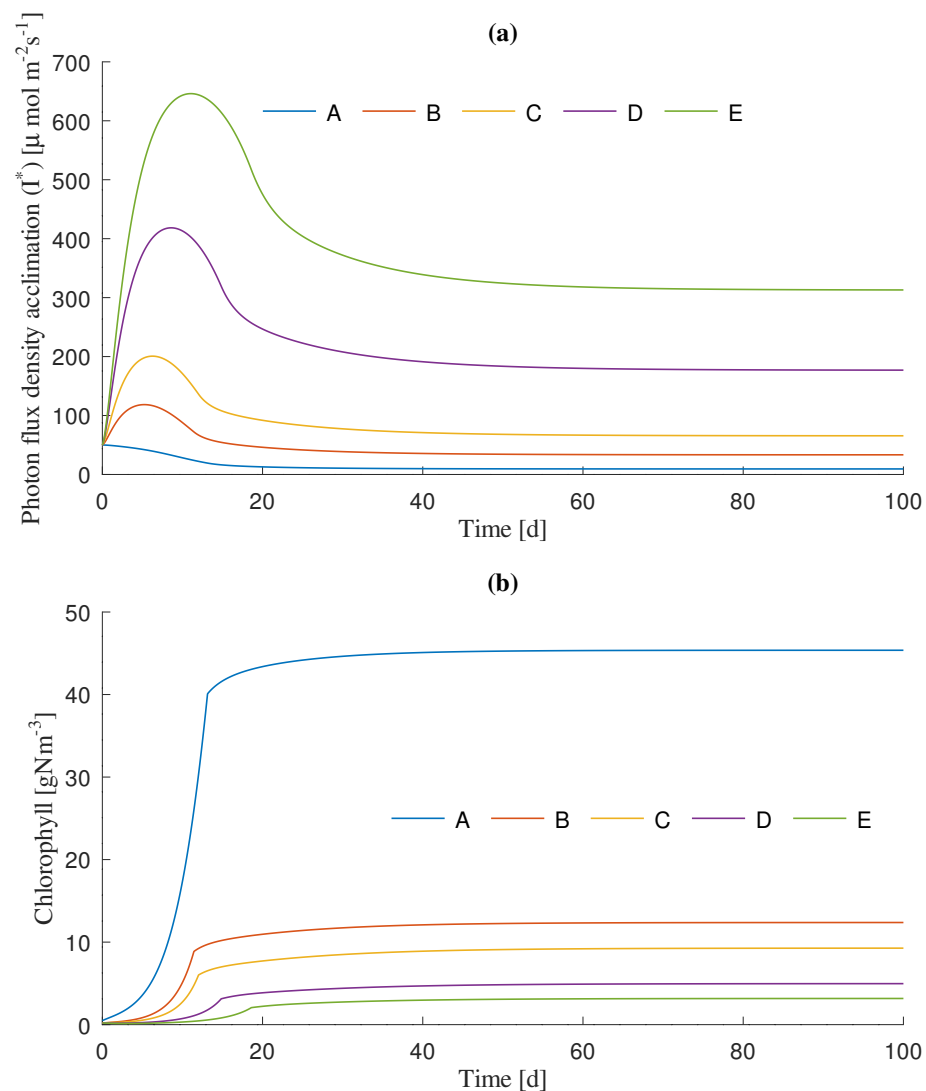
Figure 5. Simulation of (**a**) photoacclimation and (**b**) chlorophyll concentration in a continuous culture system of microalgae of the *Isochrysis galbana* strain. The simulation input parameters are presented in Table 2 and the initial conditions in Table 5. The light-intensity settings for A, B, C, D, and E correspond to 50 μmolm^{-2}s^{-1}, 150 μmolm^{-2}s^{-1}, 250 μmolm^{-2}s^{-1}, 500 μmolm^{-2}s^{-1}, and 750 μmolm^{-2}s^{-1}, respectively.

In a mathematical simulation of carbohydrate quota dynamics, light intensity was shown to influence carbohydrate production. This may be a result of the fact that light intensity alters the way in which microalgae assimilate inorganic carbon. Consequently, low light intensities lead to a reduced capacity for carbon assimilation, which increases the ability of photosynthetic organisms to fix carbon dioxide by stimulating the synthesis of chlorophyll. In such poor lighting conditions, the assimilated carbon structures are mainly used to synthesize chlorophyll rather than other organic compounds, as shown in Figure 6b. On the other hand, nitrogen starvation in the culture medium induces a decrease in the production of pigments and an increase in the production of carbohydrates. In relation to this, the authors in [79] reported an unexpected increase in carbohydrate content in the microalgal culture under nitrogen deprivation, which aligns with the findings of [80] who observed an increase in relative carbohydrate content in *Picochlorum* under nitrogen deprivation.

In relation to the decrease in pigment production, a study conducted by [65] revealed that reducing the nitrate concentration in the cultivation medium from 8 mM to 0.5 mM led to a significant reduction in total chlorophyll and carotenoid content. Specifically, the total

chlorophyll content decreased by approximately 89.4% to 83.8% (DW), while the carotenoid content decreased by 78.1% to 67.7% (DW) under different light regimes.
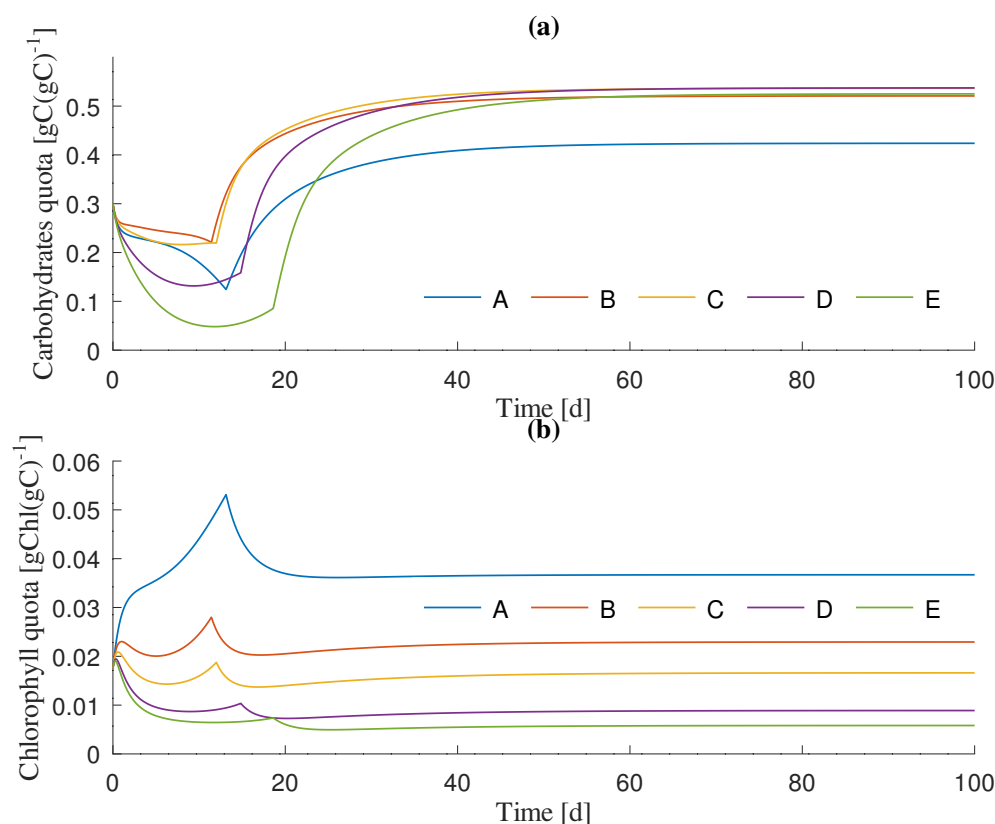

Figure 6. Simulation of (**a**) carbohydrate quota and (**b**) chlorophyll quota in a continuous culture system of microalgae of the *Isochrysis galbana* strain. The simulation input parameters are presented in Table 2 and the initial conditions in Table 5. The light intensity settings for A, B, C, D, and E correspond to 50 μmolm^{-2}s^{-1}, 150 μmolm^{-2}s^{-1}, 250 μmolm^{-2}s^{-1}, 500 μmolm^{-2}s^{-1}, and 750 μmolm^{-2}s^{-1}, respectively.

As illustrated in Figure 6a, light intensity may affect nitrogen uptake rates and delay the onset of nutrient deficiency. Studies in the literature have reported that high light intensity stress and nitrate deprivation affect the cellular metabolic activity and redirect protein synthesis toward carbohydrate accumulation [81].

It has been observed that subjecting organisms to nitrogen-deficient conditions for a short duration results in a significant elevation in carbohydrate content. This is primarily attributed to the limitation of nitrogen availability, which restricts the rate of cell division and redirects anabolic pathways away from protein synthesis toward the production of reserve substances such as carbohydrates [82–85].

Since nitrogen is an essential component of protein synthesis, its deficiency caused by high light intensities reduces protein synthesis rates. Protein synthesis is a crucial component of both the photosystem reaction center and the electron transport system in photosynthesis. Thus, since chlorophyll is a nitrogenous compound, nitrate concentration plays a significant role in the synthesis of chlorophyll. For example, in [79], it was reported that decreasing the nitrogen concentration from 144 to 0 mg/L resulted in a decrease in the concentration of *Chla* from 0.41 to 0.11 mg/L, and *Chlb* decreased from 0.56 to 0.18 mg/L.

The limitation of nitrogen adversely affects photosynthesis indirectly as well. Furthermore, chlorophyll synthesis is also controlled by the photoacclimation process [56]. The dynamic simulation revealed that high light intensity leads to a decrease in chlorophyll content. This response has been reported in the literature and is believed to be a protec-

tive mechanism to prevent the absorption of excess light energy by the photosynthetic machinery [86,87].

Based on the carbohydrate quota simulations, there was a gradual increase in carbohydrate quota as chlorophyll quotas decreased over time. This observation aligns with a study conducted by [79] who investigated the growth rate and biochemical composition of *Isochrysis galbana*. The study reported a decrease in cell growth, pigments, and protein content of I. galbana biomass as the nitrogen concentration decreased. However, under conditions of total nitrogen deprivation, the carbohydrate content reached its highest value at 47%. In another study, it was observed that the carbohydrate quota of *I. galbana* was 0.48 mgN/mgC during the initial nitrogen-sufficient growth period. However, during nitrogen starvation, the carbohydrate quota increased significantly by 87.7% [88].

Based on the aforementioned information, it can be inferred that carbohydrate production is specifically triggered when external nutrient sources have been fully depleted, as depicted in Figure 6a. This dynamic behavior is consistent with numerous studies that demonstrated that under N-limited conditions, carbohydrate contents were improved in many algal species such as *Neochloris oleoabundan* HK-129 [89], *Thermosynechococcus* sp., and *Chlorella vulgaris* [90], *Scenedesmus obliquus* CNW-N [91], *Nannochloropsis* sp., and *Tetraselmis suecica* [92].

3.2. Analysis of Productivity

Based on the methodology provided for the analysis of productivity, the following outcomes are presented.

Figure 7a illustrates the biomass productivity map based on variations in the light-intensity parameter (I_0) and the dilution rate (D).

The productivity map displays the yield of biomass concentration per unit time for the strain *Isochrysis galbana*. The equilibrium points were obtained by varying the light0intensity parameter (I_0) between 50 and 1000 $\mu mol m^{-2}s^{-1}$. The circles represent the steady state achieved multiplied by the dilution rate ($D = 0.1$). The symbol ($*$) represents the optimal point of light intensity and maximum biomass production. In terms of biomass productivity, the maximum value was 56.214 $gCm^{-3}d^{-1}$. The optimal light intensity (I_0) for maximum biomass yield was 350 $\mu mol m^{-2}s^{-1}$ under the simulation conditions proposed in this study. Biomass concentration productivity decreased when the parameter (I_0) exceeded 350 $\mu mol m^{-2}s^{-1}$. Our findings are in line with previous studies that have reported the ability of *Isochrysis galbana* to grow across a wide range of light conditions without experiencing significant stress that would require extensive cell adaptation. For instance, the literature has shown that a maximum growth rate was observed in cells grown at an irradiance level of 325 $\mu mol m^{-2}s^{-1}$, indicating the species' capability to thrive under diverse light intensities [65]. Additionally, other studies have demonstrated that the production of cell biomass in *Isochrysis galbana* cultures decreases when the light intensity exceeds 400 $\mu mol m^{-2}s^{-1}$. Conversely, increasing the light intensity from 200 to 400 $\mu mol m^{-2}s^{-1}$ leads to an increase in cell biomass. However, at intensities higher than 400 $\mu mol m^{-2}s^{-1}$, photoinhibition occurs, resulting in a decrease in cell growth. [93].

In productivity studies of *Isochrysis galbana*, Tzovenis et al. (2003) [67] reported productivities ranging from 28 to 62 $gCm^{-3}d^{-1}$ under continuous light. These values fall within the range found in our study.

Meanwhile, Figure 7b illustrates the productivity map of the biomass concentration of the strain *Isochrysis galbana* as a function of the dilution parameter (D).

This productivity map illustrates the simulation of biomass concentration per unit time of the strain *Isochrysis galbana*. The equilibrium points were determined by varying the dilution parameter (D) between 0.0125 and 0.4 d^{-1}. Circles represent the steady state reached in each simulation multiplied by the dilution rate (D) for each run between 0.0125 and 0.4 d^{-1}. Symbolically represented as ($*$), the point N(D, x) indicates the optimal point of dilution and maximum biomass production. In this study, the maximum biomass productivity was found to be 126.91 $gCm^{-3}d^{-1}$. The optimal value of dilution parameter

(*D*) for achieving maximum biomass yield was 0.325 d^{-1} under the simulation conditions described in this paper. For values of the parameter (*D*) greater than 0.325, the productivity of the biomass concentration decreased.
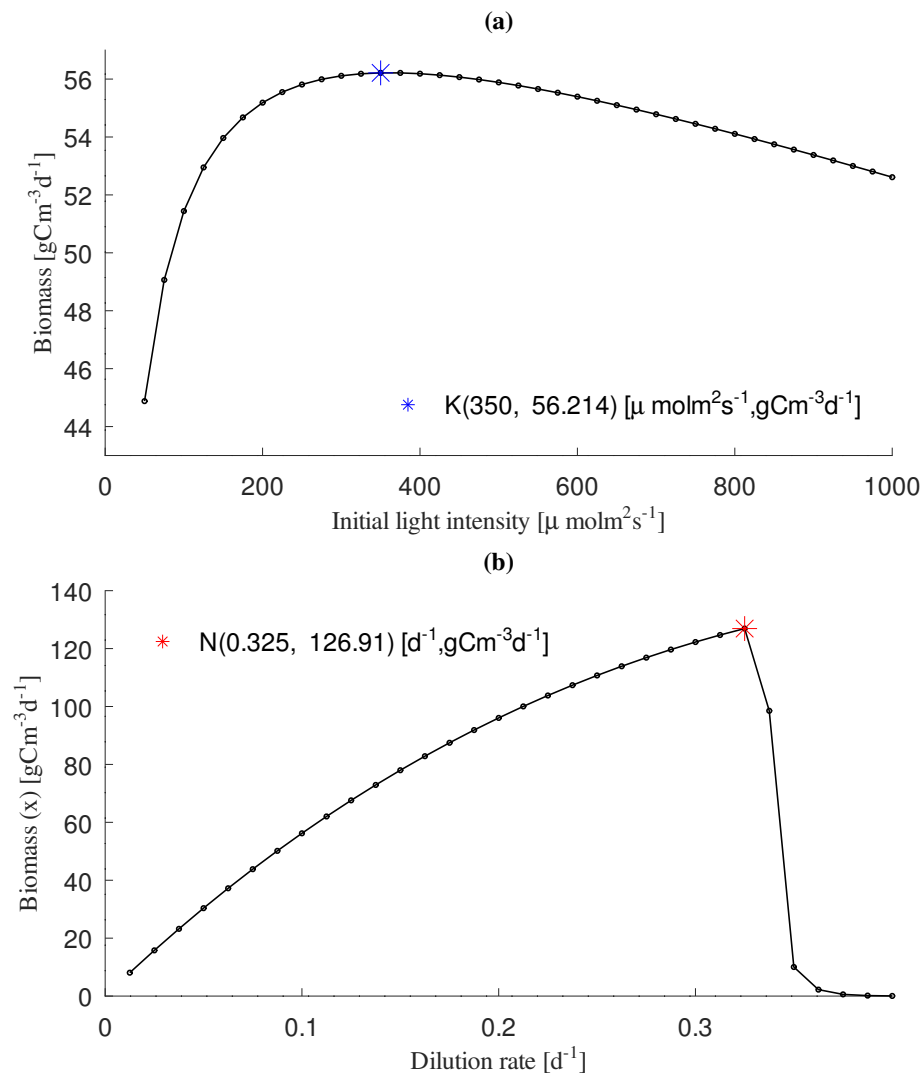
(a)

(b)

Figure 7. Steady-state productivity maps of biomass concentration with respect to (**a**) incident light intensity I_0 and (**b**) dilution rate (*D*).

Figure 8a illustrates the productivity map for the carbohydrate concentration of the strain *Isochrysis galbana* with respect to changes in the light-intensity parameter (I_0).

The productivity map shows the simulations of the concentration of carbohydrates per unit of time for the strain *Isochrysis galbana*. The equilibrium points were determined by varying the light intensity parameter (I_0) between 50 and 1000 µmolm^{-2}s^{-1}. Each circle represents the steady state achieved during each simulation multiplied by the dilution rate (*D* = 0.1). In the figure, $M(I_0,x)$ represents the optimal point of light intensity and biomass productivity, represented by the symbol (∗). As shown in Figure 8, there was a maximum carbohydrate productivity of 30.352 gCm^{-3}d^{-1}. The optimal value of the light intensity parameter (I_0) for maximum carbohydrate yield was 350 µmolm^{-2}s^{-1} under the simulation conditions that were used in this study. For values of (I_0) greater than 350 µmolm^{-2}s^{-1}, the productivity of biomass concentration decreased.

Figure 8b illustrates the productivity map of the carbohydrate concentration of strain *Isochrysis galbana* in response to changes in the dilution parameter (*D*).
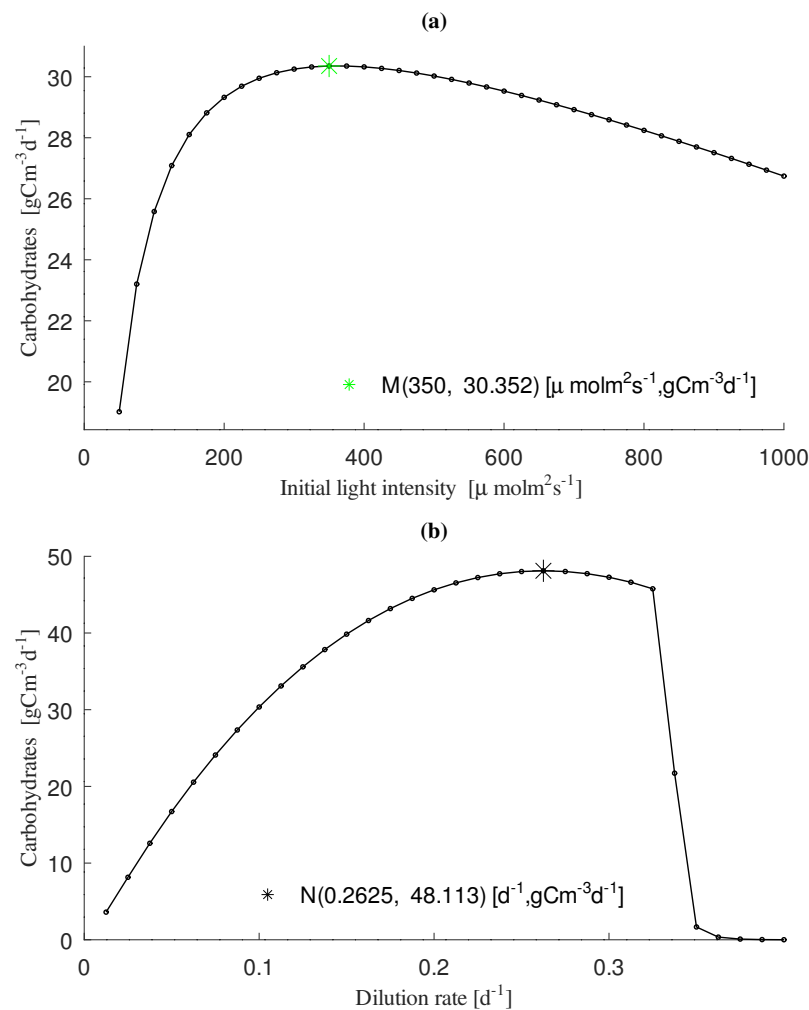
Figure 8. Steady-state productivity maps of carbohydrates concentration with respect to (**a**) incident light intensity I_0 and (**b**) dilution rate D.

The equilibrium points were determined by varying the dilution parameter (D) between 0.0125 and 0.4 d^{-1}. Each circle represents the steady state reached in each simulation multiplied by the dilution rate (D) corresponding to each run between 0.0125 and 0.4 d^{-1}. As indicated by the point $O(D, x)$ and symbol ($*$), 0.2625 d^{-1} was the optimal value of dilution rate to achieve a maximum productivity of 48.11 $gCm^{-3}d^{-1}$ under the proposed simulation conditions. Regarding this result, one study reported high sugar productivities of *I.galbana* at a dilution rate of 0.3 d^{-1} and a nitrogen concentration of 6 $gN(m^3)$ [62]. These optimal findings further highlight the significant role of nutrient deficiency in enhancing the carbohydrate content of *I.galbana*. The productivity of carbohydrates decreased for the parameter D greater than 0.2625 d^{-1}. The optimal dilution rate value was lower than that obtained from the biomass, which may be the result of the maximum storage capacity of carbohydrates under optimal operating conditions.

There is limited available data on the carbohydrate productivity of *Isochrysis galbana* in standard laboratory cultures [67]. However, carbohydrates play a crucial role as intermediate reserves in certain algae, especially when nitrogen availability becomes limited, as they are required for lipid synthesis. Studies addressing this aspect have been conducted, such as the one by [78]. They reported a carbohydrate storage of 25% in *Isochrysis galbana* strains. Moreover, during the stationary growth phase, a decrease in protein content and a slight increase in carbohydrates were observed. These findings suggest that changes in the cellular biochemical composition of I. galbana are influenced by the nutrient concentration in the medium.

3.3. Sensitivity Analysis

The system of equations below (31) is a representation of the Droop model for continuous culture systems based on the nominal parameters.

$$
\begin{aligned}
\dot{x} &= \mu(I_{0_0}, I^*, x, z, \lambda_0)x - D_0 x - R_0 x \\
\dot{y} &= Dy_{in_0} - \rho(y, z, \lambda_0)x - D_0 y \\
\dot{z} &= \rho(y, z, \lambda_0) - \bar{\mu}(I_{0_0}, I^*, x, z, \lambda_0)(z - z_{C0_0}) + R_0 z \\
\dot{g}_q &= (1 - \beta_0 z - g_q)\mu(I_{0_0}, I^*, x, z, \lambda_0) - \alpha_0 \rho(y, z, \lambda_0) + R(q_g - 1) \\
\dot{I}^* &= \mu(I_{0_0}, I^*, x, z, \lambda_0)[\bar{I}(I_0) - I^*]
\end{aligned}
\tag{31}
$$

This section describes the computation of the sensitivity equation using the arrangements (32) and (33), which summarize the Jacobian matrix elements $J_{A_{i,j}}$ and $J_{B_{i,j}}$. As n = 15 and m = 5, the matrix elements are denoted as [A(1,n)... A(m,n)], respectively.

$$
J_{A_{i,j}} = \frac{\partial f_i(x, t, \lambda)}{\partial \lambda_j} =
\begin{bmatrix}
\dfrac{\partial f_1(x, t, \lambda)}{\partial x_1} & \cdots & \dfrac{\partial f_1(x, t, \lambda)}{\partial x_n} \\
\vdots & \ddots & \vdots \\
\dfrac{\partial f_m(x, t, \lambda)}{\partial x_1} & \cdots & \dfrac{\partial f_m(x, t, \lambda)}{\partial x_n}
\end{bmatrix}
=
\begin{bmatrix}
A(1,1) & \cdots & A(1,n) \\
\vdots & \ddots & \vdots \\
A(m,1) & \cdots & A(m,n)
\end{bmatrix}
\tag{32}
$$

$$
J_{B_{i,j}} = \frac{\partial f_i(x, t, \lambda)}{\partial \lambda_j} =
\begin{bmatrix}
\dfrac{\partial f_1(x, t, \lambda)}{\partial x_1} & \cdots & \dfrac{\partial f_1(x, t, \lambda)}{\partial x_n} \\
\vdots & \ddots & \vdots \\
\dfrac{\partial f_m(x, t, \lambda)}{\partial x_1} & \cdots & \dfrac{\partial f_m(x, t, \lambda)}{\partial x_n}
\end{bmatrix}
=
\begin{bmatrix}
B(1,1) & \cdots & B(1,n) \\
\vdots & \ddots & \vdots \\
B(m,1) & \cdots & B(m,n)
\end{bmatrix}
\tag{33}
$$

In the arrangements (34) and (35), Jacobian matrices are represented by the values of the nominal parameters. The symbols ϑ y ϖ represent the elements A and B that were evaluated as nominal parameters.

$$
J_{\vartheta_{i,j}}\Big|_{\text{nominal}} =
\begin{bmatrix}
\vartheta(1,1) & \cdots & \vartheta(1,n) \\
\vdots & \ddots & \vdots \\
\vartheta(m,1) & \cdots & \vartheta(m,n)
\end{bmatrix}
\tag{34}
$$

and

$$
J_{\varpi_{i,j}}\Big|_{\text{nominal}} =
\begin{bmatrix}
\varpi(1,1) & \cdots & \varpi(1,n) \\
\vdots & \ddots & \vdots \\
\varpi(m,1) & \cdots & \varpi(m,n)
\end{bmatrix}
\tag{35}
$$

Equation (36) was used to solve the dynamic sensitivity equations numerically.

$$
\begin{aligned}
\dot{x}_1 &= f(t, x, \lambda) & x(t_0) &= x_0 \\
\dot{x}_\lambda &= \left[\frac{\partial f(t, x, \lambda)}{\partial x}\right] x_\lambda + \left[\frac{\partial f(t, x, \lambda)}{\partial \lambda}\right] & x\lambda(t_0) &= 0
\end{aligned}
\tag{36}
$$

The sensitivity equations obtained for the elements $J\vartheta_{i,j}$ and $J\varpi_{i,j}$ are shown in the supplementary materials, specifically in the arrangements (S1) and (S2). The Equations (S3)–(S102) pertaining to these elements have been included in the provided link.

A representation of the solutions to the sensitivity functions is shown in the arrangement (37). Based on the order shown in the arrangement (38) (H), each element in the arrangement (S) represents the variation in state variables as a function of a given parameter. Based on the three initial conditions shown in the Table 5, the numerical solution of the sensitivity functions was evaluated. The simulation parameters are outlined in Table 2. The simulations were carried out using the optimal values found in the productivity analysis, corresponding to a dilution rate of 0.2625 d^{-1} and a light intensity of 350 µmolm^{2}s^{-1}. In the simulation, all other parameters were kept at the same values.

$$
S = \begin{bmatrix}
x_6 & x_{11} & x_{16} & x_{21} & x_{26} & x_{31} & x_{36} & x_{41} & x_{46} & x_{51} & x_{56} & x_{61} & x_{66} & x_{71} & x_{76} \\
x_7 & x_{12} & x_{17} & x_{22} & x_{27} & x_{32} & x_{37} & x_{42} & x_{47} & x_{52} & x_{57} & x_{62} & x_{67} & x_{72} & x_{77} \\
x_8 & x_{13} & x_{18} & x_{23} & x_{28} & x_{33} & x_{38} & x_{43} & x_{48} & x_{53} & x_{58} & x_{63} & x_{68} & x_{73} & x_{78} \\
x_9 & x_{14} & x_{19} & x_{24} & x_{29} & x_{34} & x_{39} & x_{44} & x_{49} & x_{54} & x_{59} & x_{64} & x_{69} & x_{74} & x_{79} \\
x_{10} & x_{15} & x_{20} & x_{25} & x_{30} & x_{35} & x_{40} & x_{45} & x_{50} & x_{55} & x_{60} & x_{65} & x_{70} & x_{75} & x_{80}
\end{bmatrix} = H \tag{37}
$$

$$
H = \begin{bmatrix}
\frac{\partial x_1}{\partial \lambda_1} & \frac{\partial x_1}{\partial \lambda_2} & \frac{\partial x_1}{\partial \lambda_3} & \frac{\partial x_1}{\partial \lambda_4} & \frac{\partial x_1}{\partial \lambda_5} & \frac{\partial x_1}{\partial \lambda_6} & \frac{\partial x_1}{\partial \lambda_7} & \frac{\partial x_1}{\partial \lambda_8} & \frac{\partial x_1}{\partial \lambda_9} & \frac{\partial x_1}{\partial \lambda_{10}} & \frac{\partial x_1}{\partial \lambda_{11}} & \frac{\partial x_1}{\partial \lambda_{12}} & \frac{\partial x_1}{\partial \lambda_{13}} & \frac{\partial x_1}{\partial \lambda_{14}} & \frac{\partial x_1}{\partial \lambda_{15}} \\
\frac{\partial x_2}{\partial \lambda_1} & \frac{\partial x_2}{\partial \lambda_2} & \frac{\partial x_2}{\partial \lambda_3} & \frac{\partial x_2}{\partial \lambda_4} & \frac{\partial x_2}{\partial \lambda_5} & \frac{\partial x_2}{\partial \lambda_6} & \frac{\partial x_2}{\partial \lambda_7} & \frac{\partial x_2}{\partial \lambda_8} & \frac{\partial x_2}{\partial \lambda_9} & \frac{\partial x_2}{\partial \lambda_{10}} & \frac{\partial x_2}{\partial \lambda_{11}} & \frac{\partial x_2}{\partial \lambda_{12}} & \frac{\partial x_2}{\partial \lambda_{13}} & \frac{\partial x_2}{\partial \lambda_{14}} & \frac{\partial x_2}{\partial \lambda_{15}} \\
\frac{\partial x_3}{\partial \lambda_1} & \frac{\partial x_3}{\partial \lambda_2} & \frac{\partial x_3}{\partial \lambda_3} & \frac{\partial x_3}{\partial \lambda_4} & \frac{\partial x_3}{\partial \lambda_5} & \frac{\partial x_3}{\partial \lambda_6} & \frac{\partial x_3}{\partial \lambda_7} & \frac{\partial x_3}{\partial \lambda_8} & \frac{\partial x_3}{\partial \lambda_9} & \frac{\partial x_3}{\partial \lambda_{10}} & \frac{\partial x_3}{\partial \lambda_{11}} & \frac{\partial x_3}{\partial \lambda_{12}} & \frac{\partial x_3}{\partial \lambda_{13}} & \frac{\partial x_3}{\partial \lambda_{14}} & \frac{\partial x_3}{\partial \lambda_{15}} \\
\frac{\partial x_4}{\partial \lambda_1} & \frac{\partial x_4}{\partial \lambda_2} & \frac{\partial x_4}{\partial \lambda_3} & \frac{\partial x_4}{\partial \lambda_4} & \frac{\partial x_4}{\partial \lambda_5} & \frac{\partial x_4}{\partial \lambda_6} & \frac{\partial x_4}{\partial \lambda_7} & \frac{\partial x_4}{\partial \lambda_8} & \frac{\partial x_4}{\partial \lambda_9} & \frac{\partial x_4}{\partial \lambda_{10}} & \frac{\partial x_4}{\partial \lambda_{11}} & \frac{\partial x_4}{\partial \lambda_{12}} & \frac{\partial x_4}{\partial \lambda_{13}} & \frac{\partial x_4}{\partial \lambda_{14}} & \frac{\partial x_4}{\partial \lambda_{15}} \\
\frac{\partial x_5}{\partial \lambda_1} & \frac{\partial x_5}{\partial \lambda_2} & \frac{\partial x_5}{\partial \lambda_3} & \frac{\partial x_5}{\partial \lambda_4} & \frac{\partial x_5}{\partial \lambda_5} & \frac{\partial x_5}{\partial \lambda_6} & \frac{\partial x_5}{\partial \lambda_7} & \frac{\partial x_5}{\partial \lambda_8} & \frac{\partial x_5}{\partial \lambda_9} & \frac{\partial x_5}{\partial \lambda_{10}} & \frac{\partial x_5}{\partial \lambda_{11}} & \frac{\partial x_5}{\partial \lambda_{12}} & \frac{\partial x_5}{\partial \lambda_{13}} & \frac{\partial x_5}{\partial \lambda_{14}} & \frac{\partial x_5}{\partial \lambda_{15}}
\end{bmatrix} \tag{38}
$$

The solution of Equation (36) was computed for the three different initial states presented in Table 5. Figure 9 shows x_6, x_{11}, x_{16}, x_{21}, x_{26}, x_{31}, x_{36}, x_{41}, x_{46}, x_{51}, x_{56}, x_{61}, x_{66}, x_{71}, and x_{76}, which are the sensitivities of biomass concentration x_1 with respect to the parameters shown in arrangement (38). Figures 9–13 showed the corresponding sensitivities for external nutrient concentration x_2, internal quota x_3, photoacclimation x_4, and the carbohydrate quota x_5.

Inspection of these figures shows, in order of importance, that the solution of the state variables are more sensitive to variations in the parameters $\lambda_{0_{10}}$, λ_{0_7}, λ_{0_1}, and λ_{0_9} than to all other parameters evaluated; these more sensitive parameters correspond to zc_{0_0}, ρ_{m_0}, D_0, and zc_{m0}, respectively. These findings align with a previous sensitivity analysis conducted for nutrient-limited batch cultivation, which demonstrated a greater sensitivity of the model outputs to changes in the parameter associated with minimal cell quota [41]. The sensitivity analysis conducted in this study enables the identification of significant parameters and their interrelationships. Specifically, zc_{0_0}, ρ_{m_0}, and zc_{m0} are found to have a direct correlation with the nitrogen uptake rate $\rho(y, z)$. The nitrogen uptake rate represents the microalgae's ability and affinity to utilize nitrogen from its surroundings for growth and metabolism, taking into account factors such as light stress and other environmental conditions. Consequently, these parameters have a direct influence on biomass productivity. Additionally, it can be observed that the model solutions are more sensitive under the scenario of low biomass concentration and initial nutrient levels (C_1) compared to the scenarios (C_2 and C_3). Another important point is that this type of sensitivity analysis allows us to dynamically observe the effect of parameter variations on the model solutions. It provides insights into the specific growth stages of the culture where parameter variations have a more pronounced impact.

Therefore, a sensitivity analysis can help optimize the parameter adjustment of the model, enhancing its predictive capability and understanding of the underlying biological processes. The highly sensitive parameters identified in this study hold promising applications in extremum seeking control (ESC) [94], an adaptive control strategy that actively and continuously seeks optimal values of a variable in a system by adjusting system parameters based on real-time feedback to optimize performance. A dedicated investigation by [95] explored the feasibility of dynamically adjusting light intensity to consistently track optimal biomass productivity. This study aimed to achieve this objective in a nearly model-free setup, following the principles of the extremum seeking control approach. The experimental setup focused specifically on cultures of *Isochrysis galbana*, employing the model proposed by Bernard [56] and Mairet [57]. In this evaluation, the parameters associated with the influence of light (K_{iI}, K_{sI}^*, γ_m, K_I) were systematically tested and demonstrated significant effects on the system performance [95].
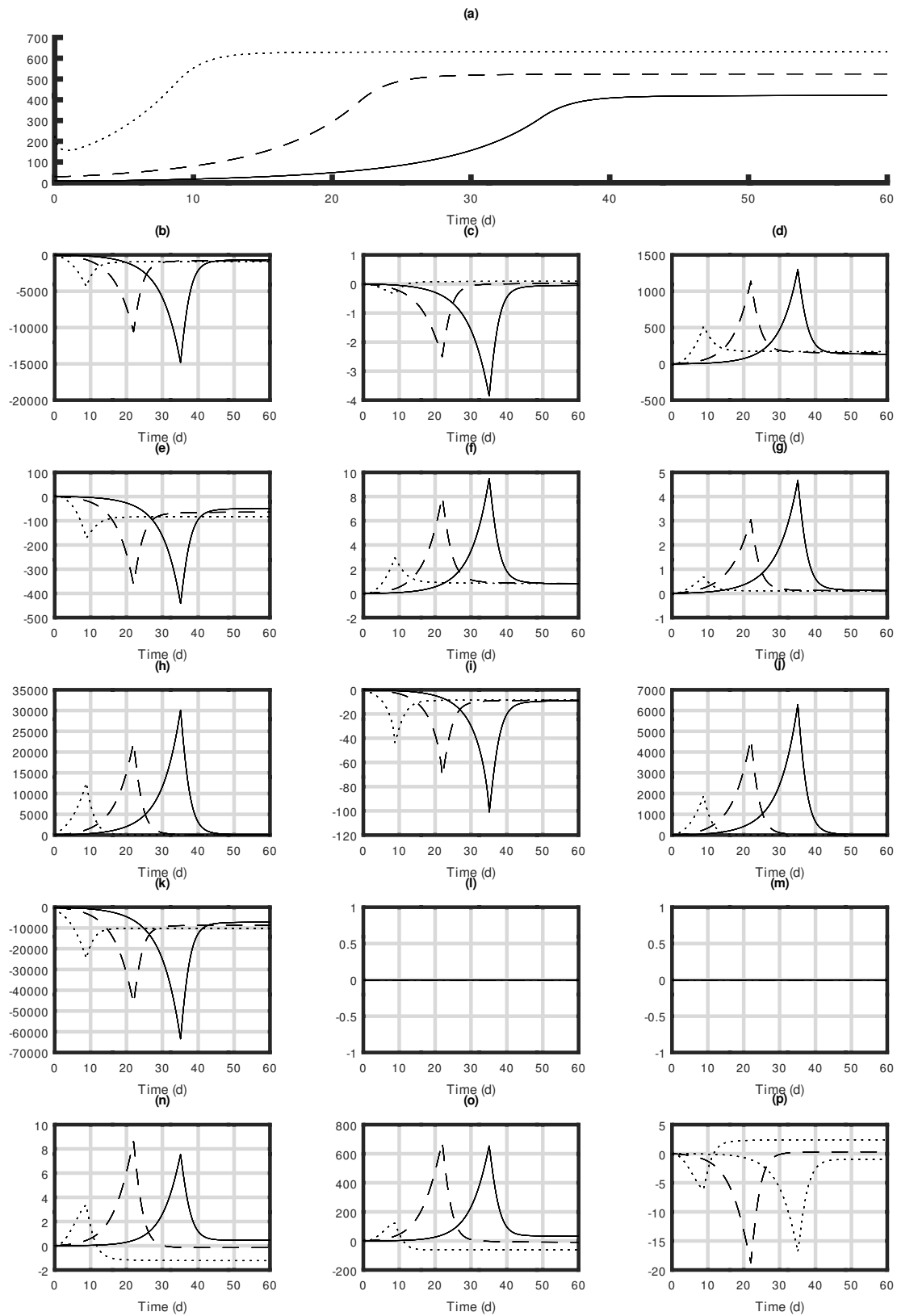
Figure 9. Sensitivity functions of (**a**) x_1 with respect to (**b**) x_6, (**c**) x_{11}, (**d**) x_{16}, (**e**) x_{21}, (**f**) x_{26}, (**g**) x_{31}, (**h**) x_{36}, (**i**) x_{41}, (**j**) x_{46}, (**k**) x_{51}, (**l**) x_{56}, (**m**) x_{61}, (**n**) x_{66}, (**o**) x_{71}, and (**p**) x_{76}. The solid line corresponds to the simulation with C_1 initial conditions, 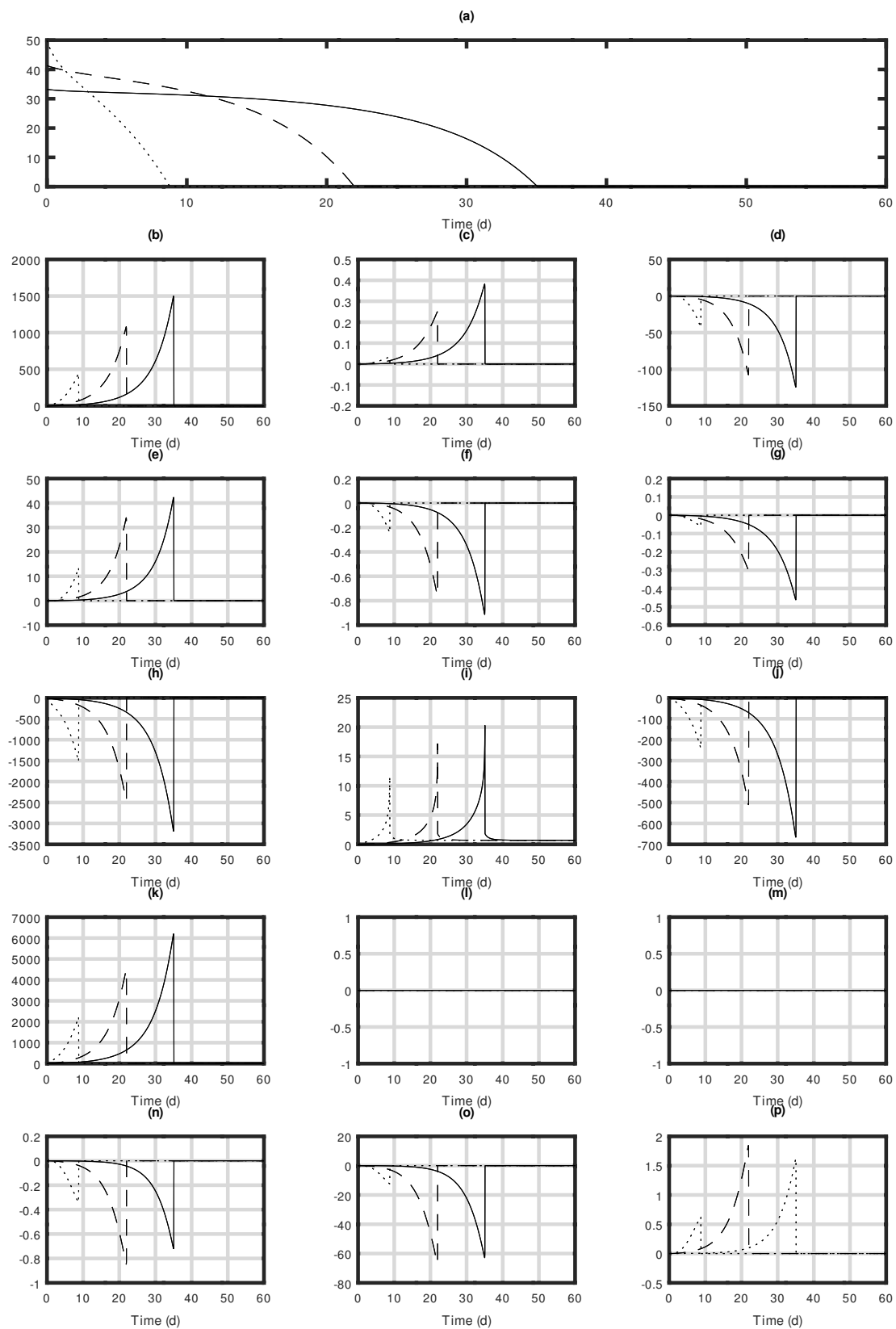the dashed line corresponds to the simulation with C_2 initial conditions, and the dotted line corresponds to the simulation with C_3 initial conditions.
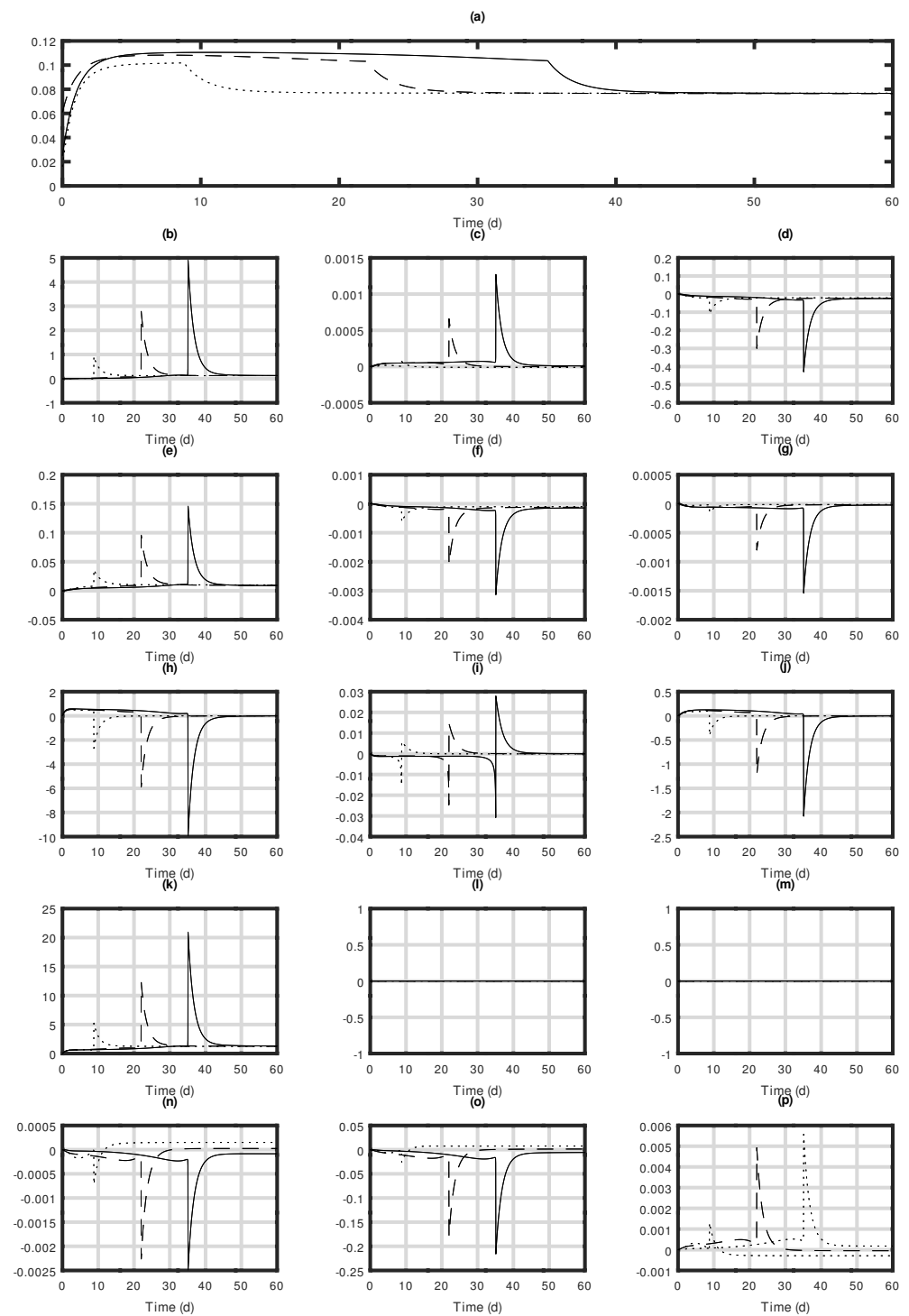
Figure 10. Sensitivity functions of (**a**) x_2 with respect to (**b**) x_7, (**c**) x_{12}, (**d**) x_{17}, (**e**) x_{22}, (**f**) x_{27}, (**g**) x_{32}, (**h**) x_{37}, (**i**) x_{42}, (**j**) x_{47}, (**k**) x_{52}, (**l**) x_{57}, (**m**) x_{62}, (**n**) x_{67}, (**o**) x_{72}, and (**p**) x_{77}. The solid line corresponds to the simulation with C_1 initial conditions, the dashed line corresponds to the simulation with C_2 initial conditions, and the dotted line corresponds to the simulation with C_3 initial conditions.
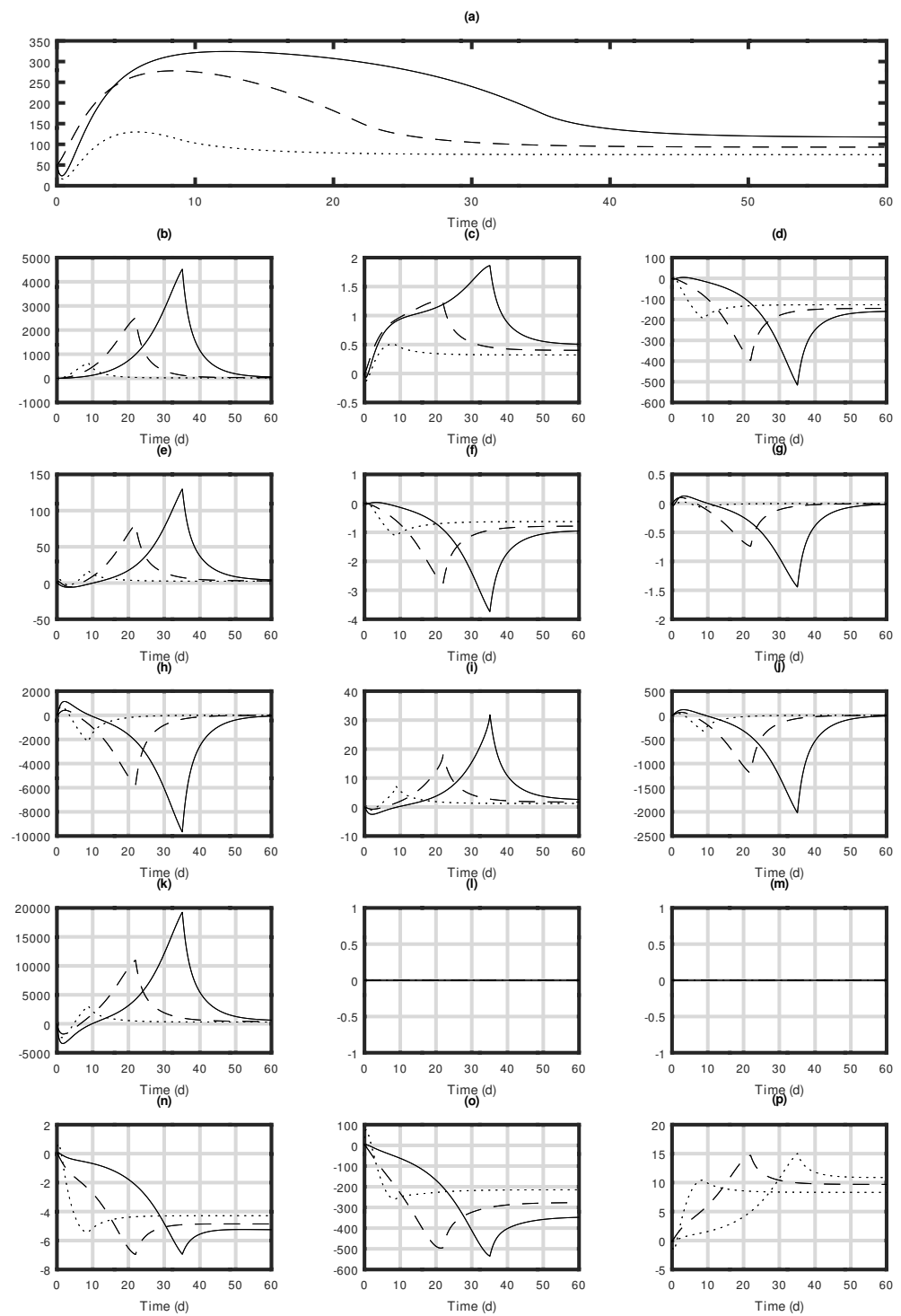
Figure 11. Sensitivity functions of (**a**) x_3 with respect to (**b**) x_8, (**c**) x_{13}, (**d**) x_{18}, (**e**) x_{23}, (**f**) x_{28}, (**g**) x_{33}, (**h**) x_{38}, (**i**) x_{43}, (**j**) x_{48}, (**k**) x_{53}, (**l**) x_{58}, (**m**) x_{63}, (**n**) x_{68}, (**o**) x_{73}, and (**p**) x_{78}. The solid line corresponds to the simulation with C_1 initial conditions, the dashed line corresponds to the simulation with C_2 initial conditions, and the dotted line corresponds to the simulation with C_3 initial conditions.
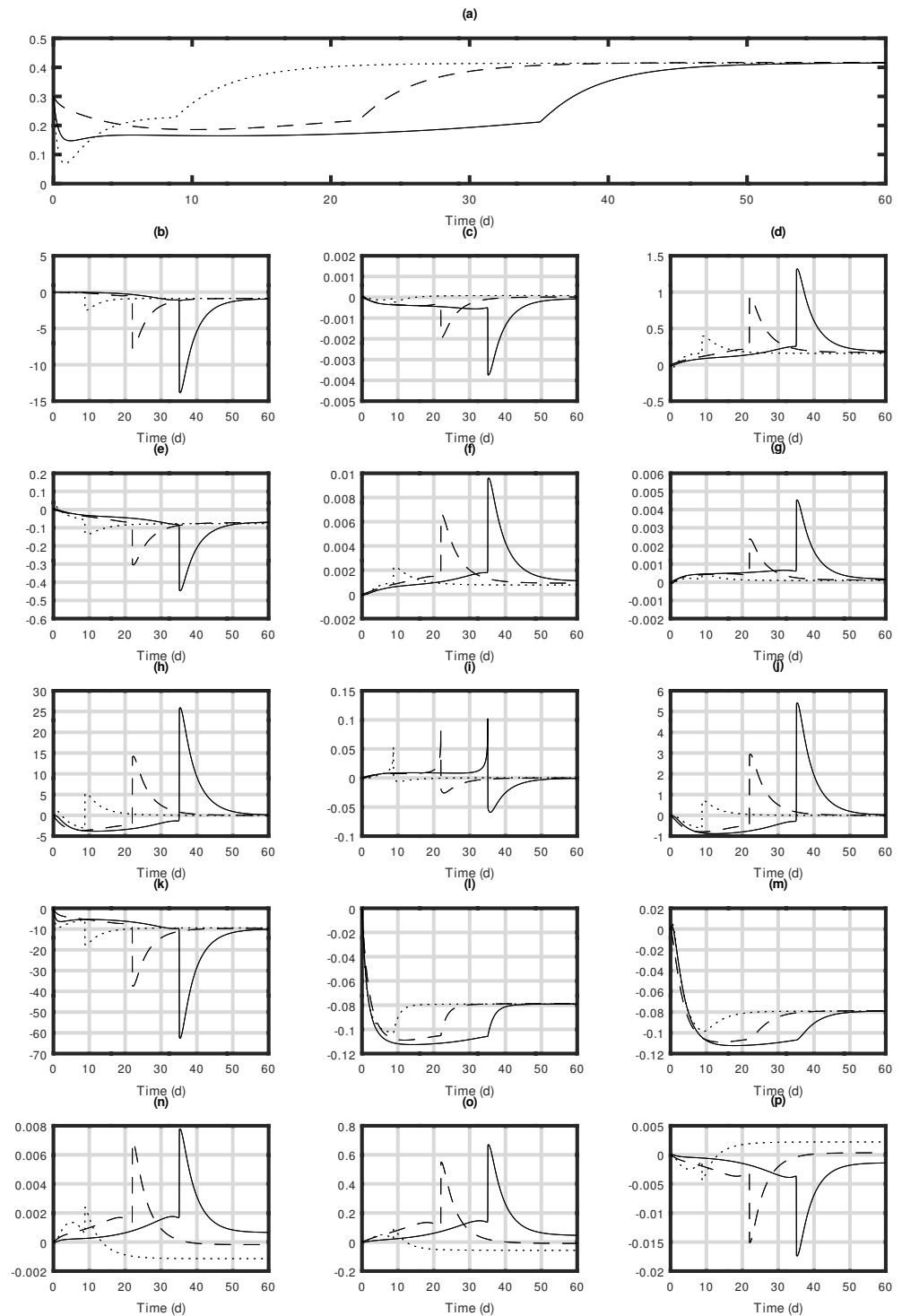
Figure 12. Sensitivity functions of (**a**) x_4 with respect to (**b**) x_9, (**c**) x_{14}, (**d**) x_{19}, (**e**) x_{24}, (**f**) x_{29}, (**g**) x_{34}, (**h**) x_{39}, (**i**) x_{44}, (**j**) x_{49}, (**k**) x_{54}, (**l**) x_{59}, (**m**) x_{64}, (**n**) x_{69}, (**o**) x_{74}, and (**p**) x_{79}. The solid line corresponds to the simulation with C_1 initial conditions, the dashed line corresponds to the simulation with C_2 initial conditions, and the dotted line corresponds to the simulation with C_3 initial conditions.

Figure 13. Sensitivity functions of (**a**) x_5 with respect to (**b**) x_{10}, (**c**) x_{15}, (**d**) x_{20}, (**e**) x_{25}, (**f**) x_{30}, (**g**) x_{35}, (**h**) x_{40}, (**i**) x_{45}, (**j**) x_{50}, (**k**) x_{55}, (**l**) x_{60}, (**m**) x_{65}, (**n**) x_{70}, (**o**) x_{75}, and (**p**) x_{80}. The solid line corresponds to the simulation with C_1 initial conditions, the dashed line corresponds to the simulation with C_2 initial conditions, and the dotted line corresponds to the simulation with C_3 initial conditions.

4. Conclusions

In this report, a dynamic photoacclimated model for continuous microalgae culture systems was used for the study of time-varying state variables under various light scenarios as well as the first-order effects of solutions to parameter variations under optimal productivity conditions. The results of this study demonstrated that the dynamic photoacclimated

model is an effective tool for studying the time-varying behavior of microalgae culture systems and can be used to identify optimal parameters to maximize productivity. Under the proposed simulation conditions, a maximum carbohydrate productivity of 48.11 $\text{gCm}^{-3}\text{d}^{-1}$ was achieved using an optimal dilution rate of 0.2625 d^{-1} and 350 $\mu\text{molm}^{-2}\text{s}^{-1}$ of light intensity. However, a particular set of manipulated inputs can generate multiple outputs at a steady state. Based on the optimal operating conditions identified as nominal parameters, sensitivity analysis was conducted. Sensitivity functions were solved to provide first-order estimates of the effect of parameter variations over time in solutions. The resulting model solutions were more sensitive to variations in the parameter of minimum nitrogen quota, maximum nitrogen intake rate, dilution rate, and maximum nitrogen uptake rate. The sensitivity pattern was consistent when solved for other initial states. Furthermore, sensitivity increased during the physiological stage of exponential growth, and the model solutions were more sensitive under conditions of low cell and nutrient concentrations. This analytical tool could be considered highly useful, as it facilitated model development, validation, and the reduction of uncertainty, ultimately enhancing the reliability of the results. Through the use of a photoacclimated model, a dynamic simulation of a continuous culture system of the strain *I. galbana* was conducted.The photoacclimation process interacts dynamically with chlorophyll synthesis, nutrient incorporation, and carbohydrate accumulation. Two independent but closely related processes for carbohydrate synthesis were observed to be affected by light: nitrogen assimilation and protein formation. Based on the underlying model, chlorophyll is proportional to cellular proteins (i.e., linearly correlated to particulate nitrogen). Furthermore, dynamic simulations have shown that microalgae cells stopped dividing as nutrient deprivation increased their carbohydrate content. Observations indicated a tradeoff between high light intensities, nitrogen assimilation, and carbohydrate synthesis. Given the interdependence between these processes and the fact that microalgae cells undergo metabolic switching from protein to carbohydrate synthesis under nitrate deprivation, excess light can delay nitrogen depletion and subsequent carbohydrate synthesis. On the other hand, low light intensities decrease chlorophyll production, resulting in insufficient energy absorption for photosynthesis. This approach could be useful for developing models suitable for optimizing industrial processes for microalgae-based carbohydrate production. Light plays an an influential role in modifying metabolic pathways as a stress factor. Combining cell stress strategies such as nutritional deficiency and light intensity regulation in order to improve carbohydrate productivity in continuous photobioreactors for microalgae cultivation. In order to quantify the impact of other factors that can cause stress to the cell, it is recommended to mathematically integrate the effects of these factors as well. This approach could be useful for developing models suitable for optimizing industrial processes for microalgae-based carbohydrate production.

Supplementary Materials: The following supporting information can be downloaded at: https://www.mdpi.com/article/10.3390/pr11071866/s1, Arrangements (S1) and (S2): Sensitivity equations obtained from the photoacclimated model utilized in this study; Equations (S3)–(S102): The elements $J\vartheta_{i,j}$ and $J\varpi_{i,j}$ of the sensitivity equations.

Institutional Review Board Statement: Not applicable.

Abbreviations

The following abbreviations are used in this manuscript:

NADPH	Nicotinamide Adenine Dinucleotide Phosphate
PBR	photobioreactor
FFA	free fatty acid
ODE	ordinary differential equation
LSODE	Livermore solver for ordinary differential equations
ATP	adenosine triphosphate

References

1. Chia, S.R.; Ong, H.C.; Chew, K.W.; Show, P.L.; Phang, S.M.; Ling, T.C.; Nagarajan, D.; Lee, D.J.; Chang, J.S. Sustainable approaches for algae utilisation in bioenergy production. *Renew. Energy* **2018**, *129*, 838–852. [CrossRef]
2. Vadiveloo, A.; Moheimani, N. Effect of continuous and daytime mixing on Nannochloropsis growth in raceway ponds. *Algal Res.* **2018**, *33*, 190–196. [CrossRef]
3. Li, Y.; Horsman, M.; Wu, N.; Lan, C.Q.; Dubois-Calero, N. Biofuels from Microalgae. *Biotechnol. Prog.* **2008**, *24*, 815–820. [CrossRef] [PubMed]
4. Mohan, D.; Pittman, C.U.; Steele, P.H. Pyrolysis of wood/biomass for bio-oil: a critical review. *Energy Fuels* **2006**, *24*, 848–89 [CrossRef]
5. Babu, S.S.; Gondi, R.; Vincent, G.S.; JohnSamuel, G.C.; Jeyakumar, R.B. Microalgae Biomass and Lipids as Feedstock for Biofuels: Sustainable Biotechnology Strategies. *Sustainability* **2022**, *14*, 15070. [CrossRef]
6. Jagadevan, S.; Banerjee, A.; Banerjee, C.; Guria, C.; Tiwari, R.; Baweja, M.; Shukla, P. Recent developments in synthetic biology and metabolic engineering in microalgae towards biofuel production. *Biotechnol. Biofuels* **2018**, *11*, 185. [CrossRef]
7. Culaba, A.B.; Ubando, A.T.; Ching, P.M.L.; Chen, W.-H.; Chang, J.-S. Biofuel from Microalgae: Sustainable Pathways. *Sustainability* **2020**, *12*, 8009. [CrossRef]
8. Kings, A.J.; Raj, R.E.; Miriam, L.R.M.; Visvanathan, M.A. Cultivation, extraction and optimization of biodiesel production from potential microalgae *Euglena sanguinea* using eco-friendly natural catalyst. *Energy Convers. Manag.* **2017**, *141*, 224–35 [CrossRef]
9. Arora, P.; Chance, R.R.; Hendrix, H.; Realff, M.J.; Thomas, V.M.; Yuan, Y. Greenhouse Gas Impact of Algal Bio-Crude Production for a Range of CO_2 Supply Scenarios. *Appl. Sci.* **2021**, *11*, 11931. [CrossRef]
10. Liu, C.M.; Sandhu, N.K.; McCoy, S.T.; Bergerson, J.A. A life cycle assessment of greenhouse gas emissions from direct air capture and Fischer-Tropsch fuel production. *Sustain. Energy Fuels* **2020**, *4*, 3129–3142. [CrossRef]
11. Guest, G.; Cherubini, F.; Strømman, A.H. Global Warming Potential of Carbon Dioxide Emissions from Biomass Stored in the Anthroposphere and Used for Bioenergy at End of Life. *J. Ind. Ecol.* **2013**, *17*, 20–30. [CrossRef]
12. Chisti, Y. Biodiesel from microalgae. *Biotechnol. Adv.* **2007**, *25*, 294–306. [CrossRef]
13. Park, S.; Ahn, Y.; Pandi, K.; Ji, M.-K.; Yun, H.-S.; Choi, J.-Y. Microalgae Cultivation in Pilot Scale for Biomass Production Using Exhaust Gas from Thermal Power Plants. *Energies* **2019**, *12*, 3497. [CrossRef]
14. Rehman, M.; Kesharvani, S.; Dwivedi, G.; Gidwani, K. Impact of cultivation conditions on microalgae biomass productivity and lipid content. *Mater. Today Proc.* **2022**, *56*, 282–290. [CrossRef]
15. Bekirogullari, M.; Figueroa-Torres, G.M.; Pittman, J.K.; Theodoropoulos, C. Models of microalgal cultivation for added-value products—A review. *Biotechnol. Adv.* **2020**, *44*, 107609. [CrossRef]
16. Pignolet, O.; Jubeau, S.; Vaca-Garcia, C.; Michaud, P. Highly valuable microalgae: Biochemical and topological aspects. *J. Ind. Microbiol. Biotechnol.* **2016**, *28*, 1453–1457. [CrossRef]
17. Mooij, P.R.; de Jongh, L.D.; van Loosdrecht, M.C.; Kleerebezem, R. Influence of silicate on enrichment of highly productive microalgae from a mixed culture. *J. Appl. Phycol.* **2013**, *40*, 781–796. [CrossRef] [PubMed]
18. Markou, G.; Depraetere, O.; Vandamme, D.; Muylaert, K. Cultivation of Chlorella vulgaris and Arthrospira platensis with recovered phosphorus from wastewater by means of zeolite sorption. *Int. J. Mol. Sci.* **2015**, *16*, 4250–4264. [CrossRef] [PubMed]
19. Yang, B.; Liu, J.; Ma, X.; Guo, B.; Liu, B; Wu, T.; Jiang, Y.; Chen, F. Genetic engineering of the Calvin cycle toward enhanced photosynthetic CO_2 fixation in microalgae. *Biotechnol. Biofuels* **2017**, *10*, 229. [CrossRef] [PubMed]

20. Silvello, M.A.D.C.; Gonçalves, I.S.; Azambuja, S.P.H.; Costa, S.S.; Silva, P.G.P.; Santos, L.O.; Goldbeck, R. Microalgae-based carbohydrates: A green innovative source of bioenergy. *Bioresour. Technol.* **2022**, *344*, 126304. [CrossRef]

21. Lam, G.P.; Giraldo, J.B.; Vermuë, M.H.; Olivieri, G.; Eppink, M.H.; Wijffels, R.H. Understanding the salinity effect on cationic polymers in inducing flocculation of the microalga Neochloris oleoabundans. *J. Biotechnol.* **2016**, *225*, 10–17 [CrossRef]

22. Lakatos, G.E.; Ranglová, K.; Manoel, J.C.; Grivalský, T.; Kopecký, J.; Masojídek, J. Bioethanol production from microalgae polysaccharides. *Folia Microbiol.* **2019**, *64*, 627–644 [CrossRef] [PubMed]

23. Dai, L.; Tan, L.; Jin, X.; Wu, H.; Houbo, W.; Tao, L.; Wenzhou, X. Evaluating the potential of carbohydrate-rich microalga *Rhodosorus* sp. SCSIO-45730 as a feedstock for biofuel and *β*-glucans using strategies of phosphate optimization and low-cost harvest. *J. Appl. Phycol.* **2020**, *32*, 3051–3061. [CrossRef]

24. Gupta, S.K.; Kumar, N.M.; Guldhe, A.; Ansari, F.A.; Rawat, I.; Nasr, M.; Bux, F. Wastewater to biofuels: Comprehensive evaluation of various flocculants on biochemical composition and yield of microalgae. *Ecol. Eng.* **2018**, *117*, 62–68. [CrossRef]

25. Andreeva, A.; Budenkova, E.; Babich, O.; Sukhikh, S.; Dolganyuk, V.; Michaud, P.; Ivanova, S. Influence of Carbohydrate Additives on the Growth Rate of Microalgae Biomass with an Increased Carbohydrate Content. *Mar. Drugs* **2021**, *19*, 381. [CrossRef] [PubMed]

26. Yen, H.W.; Hu, I.C.; Chen, C.Y.; Ho, S.H.; Lee, D.J.; Chang, J.S. Microalgae-based biorefinery—From biofuels to natural products. *Bioresour. Technol* **2012**, *135*, 166–174. [CrossRef]

27. Huang, Q.; Jiang, F.; Wang, L.; Yang, C. Design of Photobioreactors for Mass Cultivation of Photosynthetic Organisms. *Engineering* **2017**, *3*, 318–329. [CrossRef]

28. Gojkovic, Ž.; Garbayo-Nores, I.; Gómez-Jacinto, V.; García-Barrera, T.; Gómez-Ariza, J.L.; Márová, I.; Vilchez-Lobato, C. Continuous production of selenomethionine-enriched Chlorella sorokiniana biomass in a photobioreactor. *Process Biochem.* **2013**, *48*, 1235–1241. [CrossRef]

29. Sero, E.T.; Siziba, N.; Bunhu, T.; Shoko, R.; Jonathan, E. Biophotonics for improving algal photobioreactor performance: A review. *Int. J. Energy Res.* **2020**, *44*, 5071–5092. [CrossRef]

30. Albarello, A.; Simionato, D.; Morosinotto, T.; Bezzo, F. Model-Based Optimization of Microalgae Growth in a Batch Plant. *Ind. Eng. Chem. Res.* **2019**, *58*, 5121–5130. [CrossRef]

31. Guzmán, J.L.; Acién, F.G.; Berenguel, M. Modelling and control of the microalgae production in industrial photobioreactors. *Rev. Iberoam. Autom. Inf.* **2021**, *18*, 1–18.

32. Rizwan, M.; Mujtaba, G.; Memon, S.A.; Lee, K.; Rashid, N.Exploring the potential of microalgae for new biotechnology applications and beyond: A review. *Renew. Sustain. Energy Rev.* **2018**, *92*, 394–404. [CrossRef]

33. Guterman, H.; Vonshak, A.; Ben-Yaakov, S. A macromodel for outdoor algal mass production. *Biotechnol. Bioeng.* **1990**, *35*, 809–819. [CrossRef] [PubMed]

34. Wu, W.H.; Wang, F.S.; Chang, M.S. Dynamic sensitivity analysis of biological systems. *BMC Bioinform.* **2008**, *9*, S17. [CrossRef] [PubMed]

35. Formighieri, C.; Franck, F, ; Bassi R. Regulation of the pigment optical density of an algal cell: Filling the gap between photosynthetic productivity in the laboratory and in mass culture. *J. Biotechnol.* **2012**, *162*, 115–123. [CrossRef]

36. Briones-Baez, M.F.; Aguilera-Vazquez, L.; Rangel-Valdez, N.; Martinez-Salazar, A.L.; Zuñiga, C. Multi-Objective Optimization of Microalgae Metabolism: An Evolutive Algorithm Based on FBA. *Metabolites* **2022**, *12*, 603. [CrossRef]

37. Lee, E.; Jalalizadeh, M.; Zhang, Q. Growth kinetic models for microalgae cultivation: A review. *Algal Res.* **2015**, *12*, 497–512. [CrossRef]

38. Solimeno, A.; Samsó, R.; García, J. Parameter sensitivity analysis of a mechanistic model to simulate microalgae growth. *Algal Res.* **2016**, *15*, 217–223. [CrossRef]

39. Grognard, F.; Akhmetzhanov, A.R; Bernard, O. Optimal strategies for biomass productivity maximization in a photobioreactor using natural light. *Automatica* **2014**, *50*, 359–368. [CrossRef]

40. San Pedro, A.; González-López, C.V.; Acién, F.G.; Molina-Grima, E. Marine microalgae selection and culture conditions optimization for biodiesel production. *Bioresour. Technolo.* **2013**, *134*, 353–361. [CrossRef]

41. Guzmán-Palomino, A.; Aguilera-Vázquez, L.; Hernández-Escoto, H.; García-Vite, P.M. Sensitivity, Equilibria, and Lyapunov Stability Analysis in Droop's Nonlinear Differential Equation System for Batch Operation Mode of Microalgae Culture Systems. *Mathematics* **2021**, *9*, 2192. [CrossRef]

42. Alligood, K.T.; Sauer, T.; Yorke, J.A. *Chaos: An Introduction to Dynamical Systems*; Springer: Berlin/Heidelberg, Germany, 1996.

43. Anning, T.; MacIntyre, H.L.; Pratt, S.M.; Sammes, P.J.; Gibb, S.; Geider, R.J. Photoacclimation in the marine diatom *Skeletonema costatum*. *Limnol. Oceanogr.* **2000**, *45*, 1807–1817. [CrossRef]

44. Lehman, J.T.; Botkin, D.B.; Likens, G. The assumptions and rationales of a computer model of phytoplankton population dynamics. *Limnol. Oceanogr.* **1975**, *20*, 343–364. [CrossRef]

45. Geider, R.; MacIntyre, H.; Kana, T. A dynamic regulatory model of phytoplanktonic acclimation to light, nutrients, and temperature. *Limnol. Oceanogr.* **1998**, *43*, 679–694. [CrossRef]

46. Pahlow, M. Linking chlorophyll-nutrient dynamics to the Redfield N:C ratio with a model of optimal phytoplankton growth. *Mar. Ecol. Prog. Ser.* **2005**, *287*, 33–43. [CrossRef]

47. Faugeras, B.; Bernard, O.; Sciandra, A.; Levy, M. A mechanistic modelling and data assimilation approach to estimate the carbon/chlorophyll and carbon/nitrogen ratios in a coupled hydrodynamical-biological model. *Nonlinear Process. Geophys.* **2004**, *11*, 515–533. [CrossRef]

48. Flynn, K. A mechanistic model for describing dynamic multi-nutrient, light, temperature interactions in phytoplankton. *J. Plankton Res.* **1991**, *23*, 977–997. [CrossRef]

49. Zonneveld, C. A cell-based model for the chlorophyll a to carbon ratio in phytoplankton. *Ecol. Model.* **1998**, *113*, 55–70. [CrossRef]

50. MacIntyre, H.; Kana, T.; Anning, T.; Geider, R. Photoacclimation of photosynthesis irradiance response curves and photosynthetic pigments in microalgae and cyanobacteria. *J. Phycol.* **2002**, *38*, 17–38. [CrossRef]

51. Peeters, J.C.H.; Eilers, P.H.C. The relationship between light intensity and photosynthesis—A simple mathematical model. *Hydrobiol. Bull.* **1978**, *12*, 134–136. [CrossRef]

52. Eilers, P.H.C.; Peeters, J.C.H. A model for the relationship between light intensity and the rate of photosynthesis in phytoplankton. *Ecol. Model.* **1988**, *42*, 199–215. [CrossRef]

53. Hartmann, P.; Nikolaou, A.; Chachuat, B.; Bernard, O. A Dynamic Model Coupling Photoacclimation and Photoinhibition in Microalgae. In Proceedings of the 12th European Control Conference, Zürich, Switzerland, 17–19 July 2013; Institute of Electrical and Electronics Engineers: Zürich, Switzerland, 2013; pp. 4178–4183.

54. Droop, M.R. The kinetics of uptake, growth and inhibition in *monochrysis lutheri*. *J. Mar. Biol. Assoc.* **1968**, *48*, 689–733. [CrossRef]

55. Benavides, M.; Hantson, A.-L.; Van Impe, J.F.M.; Vande Wouwer, A. Parameter identification of Droop model: An experimental case study. *Bioprocess Biosyst. Eng.* **2015**, *38*, 1783–1793. [CrossRef] [PubMed]

56. Bernard, O. Hurdles and challenges for modelling and control of microalgae for CO_2 mitigation and biofuel production. *J. Process Control* **2011**, *21*, 1378–1389. [CrossRef]

57. Mairet, F.; Bernard, O.; Masci, P.; Lacour, T.; Sciandra, A. Modelling neutral lipid production by the microalga *Isochrysis aff. galbana* under nitrogen limitation. *Bioresour. Technol.* **2011**, *102*, 142–149. [CrossRef]

58. Gorrini, F.A.; Zamudio Lara, J.M.; Biagiola, S.I.; Figueroa, J.L.; Hernández Escoto, H.; Hantson, A.-L.; Vande Wouwer, A. Experimental Study of Substrate Limitation and Light Acclimation in Cultures of the Microalgae Scenedesmus obliquus—Parameter Identification and Model Predictive Control. *Processes* **2020**, *8*, 1551. [CrossRef]

59. Eilers, P.H.C.; Peeters, J.C.H. Dynamic behaviour of a model for photosynthesis and photoinhibition. *Ecol. Model.* **1993**, *69*, 113–133. [CrossRef]

60. Bernard, O.; Masci, P.; Sciandra, A. A Photobioreactor Model in Nitrogen Limited Conditions. In Proceedings of the 6th Vienna International Conference on Mathematical Modelling, Vienna, Austria, 11–13 February 2009; European Mathematical Society: Helsinki, Finland, 2009; pp. 1521–1530.

61. Hindmarsh, A.C. ODEPACK, a Systematized Collection of ODE Solvers. In *Scientific Computing*; North-Holland: Amsterdam, The Netherlands, 1983; pp. 55–64

62. Mairet, F.; Bernard, O.; Lacour, T.; Sciandra, A. Modelling microalgae growth in nitrogen limited photobiorector for estimating biomass, carbohydrate and neutral lipid productivities. *IFAC Proc. Vol.* **2011**, *44*, 10591–10596. [CrossRef]

63. Khalil, H. *Nonlinear Systems*, 2nd ed.; Prentice-Hall: Hoboken, NJ, USA, 1996.

64. Martínez, C.; Mairet, F.; Bernard, O.; Dynamics of the periodically forced light-limited Droop model . *J. Differ. Equ.* **2020**, *269*, 3890–3913. [CrossRef]

65. Mishra, N.; Mohan, S.; Mishra, N. Influence of High Light Intensity and Nitrate Deprivation on Growth and Biochemical Composition of the Marine Microalgae *Isochrysis galbana* . *Braz. Arch. Biol. Technol.* **2019**, *62*. [CrossRef]

66. Sukenik, A.; Wahnon, R. Biochemical quality of marine unicellular algae with special emphasis on lipid composition : I. *Isochrysis galbana Aquaculture* **1991**, *97*, 61–72. [CrossRef]

67. Tzovenis, I.; De Pauw, N.; Sorgeloos, P. Optimisation of T-Iso biomass production rich in essential fatty acids: I. Effect of different light regimes on growth and biomass production. *Aquaculture.* **2003**, *216*, 203–222. [CrossRef]

68. Dayananda, C.; Sarada, R.; Usha Rani, M.; Shamala, T.R.; Ravishankar, G.A. Autotrophic cultivation of *Botryococcus braunii* for the production of hydrocarbons and exopolysaccharides in various media. *Biomass Bioenergy* **2007**, *31*, 87–93. [CrossRef]

69. Mandal, S.; Mallick, N. Microalga *Scenedesmus obliquus* as a potential source for biodiesel production. *Appl. Microbiol. Biotechnol.* **2009**, *84*, 281–291. [CrossRef] [PubMed]

70. Huppe, H.C.; Turpin, D.H.; Integration of Carbon and Nitrogen Metabolism in Plant and Algal Cells. *Annu. Rev. Plant Physiol. Plant Mol. Biol.* **1994**, *45*, 577–607. [CrossRef]

71. Liu, N.; Li, F.; Ge, F.; Tao, N.; Zhou, Q.; Wong, M. Mechanisms of ammonium assimilation by Chlorella vulgaris F1068: Isotope fractionation and proteomic approaches. *Bioresour. Technol.* **2015**, *190*, 307–314. [CrossRef]

72. Cai, T.; Park, S.Y.; Li, Y. Nutrient recovery from wastewater streams by microalgae: status and prospects. *Renew. Sustain. Energy Rev.* **2013**, *19*, 360–369. [CrossRef]

73. Hu, Q. Environmental effects on cell composition. In *Handbook of Microalgal Culture. Applied Phycology and Biotechnology*, 2nd ed.; Richmond, A., Hu, Q., Eds.; Wiley Blackwell: West Sussex, UK, 2013; pp. 114–122.

74. Li, Y.; Horsman, M.; Wang, B.; Wu, N.; Lan, C.Q. Effect of nitrogen source on cell growth and lipid accumulation of green alga Neochloris oleoabundans. *Appl. Microbiol. Biotechnol.* **2008**, *81*, 629–636. [CrossRef] [PubMed]

75. Simionato, D.; Block, M.A.; La Rocca, N.; Jouhet, J.; Maréchal, E.; Finazzi, G.; Morosinotto, T. The response of *Nannochloropsis gaditana* to nitrogen starvation includes de novo biosynthesis of triacylglycerols, a decrease of chloroplast galactolipids, and reorganization of the photosynthetic apparatus. *Eukaryot. Cell* **2013**, *12*, 665–676. [CrossRef] [PubMed]

76. Saha, S.K.; Uma, L.; Subramanian, G. Nitrogen stress induced changes in the marine cyanobacterium *Oscillatoria willei* BDU 130511. *FEMS Microbiol. Ecol.* **2006**, *45*, 263–272. [CrossRef]

77. Serpa, R.; Calderón, A. Efecto de diferentes fuentes de nitrógeno en el contenido de carotenoides y clorofila de cuatro cepas peruanas de *Dunaliella salina* TEOD. *J. Appl. Ecol.* **2006**, *5*, 93–99. [CrossRef]

78. Valenzuela-Espinoza, E.; Millán-Núñez, R.; Núñez-Cebrero, F. Protein, carbohydrate, lipid and chlorophyll a content in *Isochrysis* aff. *galbana* (clone T-Iso) cultured with a low cost alternative to the f/2 medium. *Aquac. Eng.* **2002**, *25*, 207–216. ISSN 0144-8609. [CrossRef]

79. Zarrinmehr, M. J.; Farhadian, O.; Heyrati, F. P.; Keramat, J.; Koutra, E.; Kornaros, M.; Daneshvar, E. Effect of nitrogen concentration on the growth rate and biochemical composition of the microalga, *Isochrysis galbana*. *Egypt. J. Aquat. Res.* **2020**, *46*, 153–158. [CrossRef]

80. El-Kassas, H.Y. Growth and fatty acid profile of the marine microalga *Picochlorum* sp. grown under nutrient stress conditions. *Egypt. J. Aquat. Res.* **2013**, *39*, 233–239. [CrossRef]

81. Courchesne, N.M.D.; Parisien, A.; Wang, B.; Lan, C.Q. Enhancement of lipid production using biochemical, genetic, and transcription factor engineering approaches. *J. Biotechnol.* **2009**, *141*, 31–41. [CrossRef] [PubMed]

82. Silva, A.F.; Lourenço, S.O.; Chaloub, R.M. Effects of nitrogen starvation on the photosynthetic physiology of a tropical marine microalga *Rhodomonas* sp. (Cryptophyceae). *Aquat. Bot.* **2009**, *91*, 291–297. [CrossRef]

83. Tan, K.W.; Lee, Y.K. The dilemma for lipid productivity in green microalgae: importance of substrate provision in improving oil yield without sacrificing growth. *Biotechnol. Biofuels* **2016**, *9*, 255. [CrossRef]

84. Siaut, M.; Cuiné, S.; Cagnon, C.; Fessler, B.; Nguyen, M.; Carrier, P.; Beyly, A. Oil accumulation in the model green alga *Chlamydomonas reinhardtii*: characterization, variability between common laboratory strains, and relationship with starch reserves. *BMC Biotechnol.* **2011**, *11*, 7. [CrossRef] [PubMed]

85. Praveen kumar, R.; Shameera, K.; Mahalakshmi, G.; Akbarsha, M.A.; Thajuddin, N. Influence of nutrient deprivations on lipid accumulation in a dominant indigenous microalga *Chlorella* sp: Evaluation for biodiesel production. *Biomass Bioenergy* **2012**, *37*, 60–66. [CrossRef]

86. Sánchez Saavedra, M.P.; Voltolina, D. Effect of photon fluence rates of white and blue-green light on growth efficiency and pigment content of three diatom species in batch cultures. *Cienc. Mar.* **2002**, *28*, 273–279. [CrossRef]

87. Ak, I. Effects of light intensity, salinity and temperature on growth in CAMALT1 strain of *Dunaliella viridis* Teodoresco from Turkey. *J. Biol. Sci.* **2008**, *8*, 1356–1359. [CrossRef]

88. Lacour, T.; Sciandra, A.; Talec, A.; Mayzaud, P.; Bernard, O. Neutral lipid and carbohydrate productivities as a response to nitrogen status in *isochrysis* sp. (t-iso; haptophyceae): starvation versus limitation. *J. Phycol.* **2012**, *48*, 647–656. [CrossRef] [PubMed]

89. Sun, X.; Cao, Y.; Xu, H.; Liu, Y.; Sun, J.; Qiao, D.; Cao, Y. Effect of nitrogen-starvation, light intensity and iron on triacylglyceride/carbohydrate production and fatty acid profile of Neochloris oleoabundans HK-129 by a two-stage process. *Bioresour. Technol.* **2014**, *155*, 204–212. [CrossRef]

90. Ho, S.H.; Huang, SW, Chen, C.Y.; Hasunuma, T.; Kondo, A.; Chang, J.S. Characterization and optimization of carbohydrate production from an indigenous microalga Chlorella vulgaris FSP-E. *Bioresour. Technol.* **2013**, *135*, 157–65. [CrossRef]

91. Chu, F.F.; Chu, P.N.; Shen, X.F.; Lam, P.K.; Zeng, R.J. Effect of phosphorus on biodiesel production from Scenedesmus obliquus under nitrogen-deficiency stress. *Bioresour. Technol.* **2014**, *152*, 241–6. [CrossRef] [PubMed]

92. Biondi, N.; Cheloni, G.; Tatti, E.; Decorosi, F.; Rodolfi, L.; Giovannetti, L.; Viti, C.; Tredici, M.R.; The bacterial community associated with Tetraselmis suecica outdoor mass cultures. *J. Appl. Phycol.* **2017**, *29*, 67–78. [CrossRef]

93. Che, C.A.; Kim, S.H.; Hong, H.J.; Kityo, M.K.; Sunwoo, I.Y.; Jeong, G.T.; Kim, S.K. Optimization of light intensity and photoperiod for *Isochrysis galbana* culture to improve the biomass and lipid production using 14-L photobioreactors with mixed light emitting diodes (LEDs) wavelength under two-phase culture system. *Bioresour. Technol.* **2019**, *285*, 121323. [CrossRef] [PubMed]

94. Ariyur, K.B.; Krstić, M. *Real-Time Optimization by Extremum-Seeking Control*; John Wiley and Sons: Hoboken, NJ, USA, 2003.

95. Deschênes, J.S.; Wouwer, A.V. Dynamic Optimization of Biomass Productivity in Continuous Cultures of Microalgae *Isochrysis galbana* through Modulation of the Light Intensity. *IFAC-PapersOnLine* **2015**, *48*, 1093–1099.